Proceedings of ICRC 2001: 1 © Copernicus Gesellschaft 2001

ICRC 2001

Stellar Sources of the Interstellar Medium

F.-K. Thielemann[1], D. Argast[1], F. Brachwitz[1], G. Martinez-Pinedo[1], R. Oechslin[1], T. Rauscher[1], W.R. Hix[2], M. Liebendörfer[2], A. Mezzacappa[2], P. Höflich[3], K. Iwamoto[4], K. Nomoto[5], H. Schatz[6], M.C. Wiescher[7], K.-L. Kratz[8], B. Pfeiffer[8], and S. Rosswog[9]

[1]Dept. of Physics & Astronomy, University of Basel, Klingelbergstrasse 82, CH-4056 Basel, Switzerland
[2]Physics Division, Oak Ridge National Laboratory, Oak Ridge, TN 37831-6371, USA
[3]Department of Astronomy, University of Texas, Austin, TX 78712, USA
[4]Department of Physics, Nihon University, Tokyo 101, Japan
[5]Department of Astronomy, University of Tokyo, Tokyo 113-033, Japan
[6]National Superconducting Cyclotron Laboratory & Department of Physics and Astronomy, Michigan State University, East Lansing, MI 48824
[7]Department of Physics, University of Notre Dame, Notre Dame, IN 46556, USA
[8]Institut für Kernchemie, Univ. Mainz, Fritz-Strassmann-Weg 2, D-55099 Mainz, Germany
[9]Department of Physics and Astronomy, University of Leicester, University Road, LE1 7RH, Leicester, UK

Abstract. With the exception of the Big Bang, responsible for ^{1,2}H, ^{3,4}He, and ^{7}Li, stars act as sources for the composition of the interstellar medium. Cosmic rays are related to the latter and very probably due to acceleration of the mixed interstellar medium by shock waves from supernova remnants. Thus, the understanding of the abundance evolution in the interstellar medium and especially the enrichment of heavy elements, as a function of space and time, is essential. It reflects the history of star formation and the lifetimes of the diverse contributing stellar objects. Therefore, the understanding of the endpoints of stellar evolution is essential as well. These are mainly planetary nebulae and type II/Ib/Ic supernovae as evolutionary endpoints of single stars, but also events in binary systems can contribute, like e.g. supernovae of type Ia, novae and possibly X-ray bursts and neutron star or neutron star - black hole mergers. Despite many efforts, a full and self-consistent understanding of supernovae (the main contributors to nucleosynthesis in galaxies) is not existing, yet. Their fingerprints, however, seen either in spectra, lightcurves, radioactivities/decay gamma-rays or in galactic evolution, can help to constrain the composition of their ejecta and related model uncertainties.

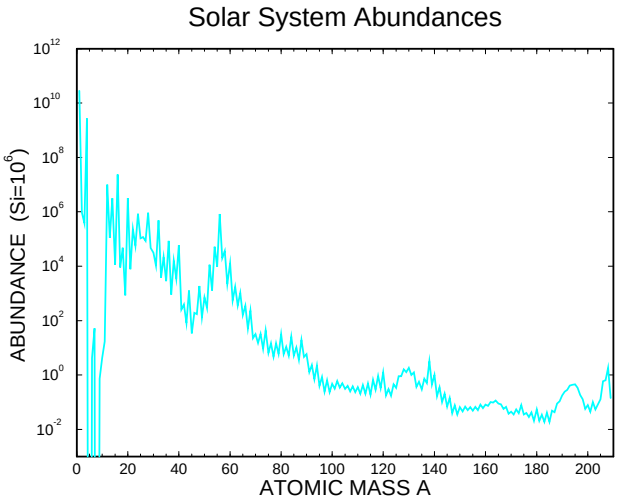

Fig. 1. Abundances by number as found in the solar system from meteorite samples and solar spectra (Grevesse & Sauval 1998). Isotopic abundances of different elements for the same mass number A are added. The units are scaled arbitrarily to a Si-abundance of Si of 10^6.

1 Introduction

The chemical composition of the interstellar medium in galaxies acts as a witness of its stellar sources. The abundances found in the solar system (shown in Fig. 1) are just a specific superposition of their yields, representing a snapshot in space and time. Galactic evolution includes variations of the weigths in this superposition, related to the evolutionary time scales of the individual contributing stellar objects. It reflects also possible variations of the individual yields as a function of metallicity.

Planetary nebulae, the endpoints of stars with M<8M$_\odot$, do contribute to light elements and heavy s-process nuclei up to Pb and Bi. These are either products of H- and He-burning (mainly ^{4}He, ^{14}N, ^{12}C, [^{16}O, ^{22}Ne]) or results of a sequence of (slow) neutron captures and beta-decays (the s-process), acting on pre-existing heavier nuclei in environments with small neutron densities. The required neutrons are provided by (α, n)-reactions in He-burning.

The evolution of the elements in the range O through Ni is dominated by two alternative explosive stellar sources, i.e. by the combined action of type II and type Ia supernovae (SNe II and Ia). SNe II, originating from massive stars (M>8M$_\odot$), leave a central neutron star and expell large amounts of the so-called alpha elements O, Ne, Mg, Si, S, Ar, Ca, Ti. Oxygen yields can be of the order 1M$_\odot$ or more while smaller amounts of Fe (and Fe-group elements like Cr, Mn, Fe, Co, Ni, Cu, Zn, Ga, Ge), typically about 0.1M$_\odot$, are produced

Correspondence to: fkt@quasar.physik.unibas.ch

in the innermost ejected mass zones. SNe Ia originate from those intermediate to low mass stars (M<8M$_\odot$) which end as mass accreting white dwarfs in binary stellar systems with high mass accretion rates (>10^{-8} M$_\odot$ y^{-1}). In that case they experience stable hydrogen and helium shell burning of the accreted matter, leading to a growing C/O white dwarf mass which approaches the Chandrasekhar mass. This causes contraction and a complete disruption of the white dwarf after carbon is ignited in the center. Predominantly Fe-group elements are produced, on average of the order 0.6-0.8 M$_\odot$, and smaller amounts of Si, S, Ar, and Ca.

Novae, the other possible endpoint of mass accreting white dwarfs in binary systems, occur for lower accretion rates. The unburned accreted hydrogen layer is ignited explosively. This causes only the ejection of the explosively processed hydrogen envelope of the order of $10^{-5} - 10^{-4}$M$_\odot$ and contributes relatively small amounts of matter to galactic evolution, mainly ^{15}N, ^{17}O and a number of specific isotopes in the range Ne through S. Type I X-ray bursts work in a similar way on accreting neutron stars in binary systems. The envelope masses involved are even smaller ($\approx 10^{-9}$M$_\odot$) and an ejection is not even clear due to the large gravitational field involved. However, in case some matter can escape it would contain interesting products from the rp-process (combined explosive hydrogen and helium burning with rapid proton captures), including the so-called light p-process isotopes of Se, Kr, Sr, Mo, and Ru.

The site for the production of the heaviest elements up to U and Th (the r-process based on rapid neutron captures in environments with very high neutron densities) is still debated and most probably related to type II supernovae and/or neutron star ejecta (from binary mergers or jets).

In the following sections 2 through 6 we want to present the status of understanding for most of these objects, including especially supernova calculations, important features in their progenitor evolution, the related nucleosynthesis and ejecta composition. Finally, in section 7, these stellar ejecta compositions will be tested for their agreement with the chemical evolution of our Galaxy.

2 Stellar Evolution and Wind Ejecta

H-burning converts ^{1}H into ^{4}He via pp-chains or the CNO-cycles. The simplest PPI chain is initiated by ^{1}H(p,$e^+\nu$)^{2}H (p,γ)^{3}He and completed by ^{3}He(^{3}He,2p)^{4}He. The dominant CNOI-cycle chain , ^{12}C(p,γ)^{13}N($e^+\nu$) ^{13}C(p,γ)^{14}N(p,γ)^{15}O ($e^+\nu$)^{15}N(p,α)^{12}C, is controlled by ^{14}N(p,γ)^{15}O, the slowest reaction of the cycle. Further burning stages are characterized by their major reactions, which are in He-burning ^{4}He($2\alpha,\gamma$)^{12}C (triple-alpha) and ^{12}C(α,γ)^{16}O, in C-burning ^{12}C(^{12}C, α)^{20}Ne, and in O-burning ^{16}O(^{16}O,α)^{28}Si (e.g. Arnett & Thielemann 1985, Thielemann & Arnett 1985, Woosley & Weaver 1995). The alternative to fusion reactions are photodisintegrations which start to play a role at sufficiently high temperatures when $30kT \approx Q$ (the Q-value or energy release of the inverse capture reaction). This ensures the existence

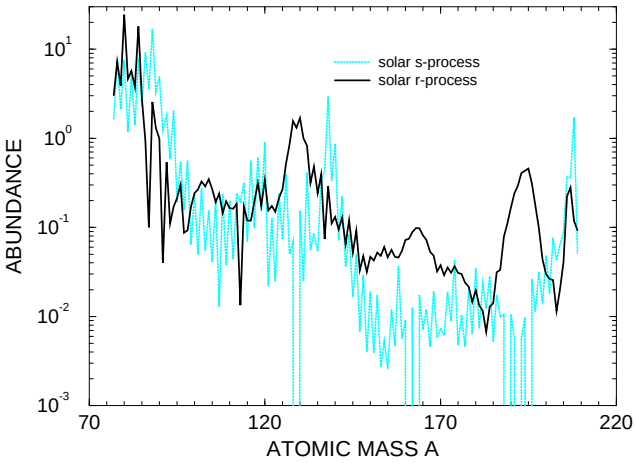

Fig. 2. Decompositions of s-process and r-process abundances (Käppeler et al. 1989, Käppeler 1999). Notice the opposite behavior of the two processes with respect to odd-even staggering as a function of mass number A.

of photons with energies $E_\gamma > Q$ in their Planck distribution and leads to Ne-Burning [^{20}Ne(γ,α)^{16}O, ^{20}Ne(α,γ)^{24}Mg] at T>1.5 $\times$ 10^9K (preceding O-burning) due to a small Q-value of ≈4 MeV and Si-burning at temperatures in excess of 3×10^9K (initiated like Ne-burning by photodisintegrations, here of ^{28}Si). The latter ends in a chemical equilibrium with an abundance distribution around Fe (nuclear statistical equilibrium, NSE) (Hix & Thielemann 1996, 1999).

While this concept and the calculational details were unquestioned in wide areas of the astrophysical community, the solar neutrino problem was still shedding doubts on the quantitative understanding of stellar evolution. The SNO experiment combined with SuperKamiokande data (Ahmad et al. 2001) gave clear evidence for neutrino conversions, explaining the missing electron neutrinos from the sun. This, together with constraints from helioseismology (Bahcall et al. 2001) gives strong support for our understanding of stellar evolution. But it has to be realized that the role of convection and its correct multi-D treatment (Asida & Arnett 2000) as well as stellar rotation, adding important features via diverse mixing processes (Heger et al. 2000ab, Meynet & Maeder 2000), need further refinement. Furthermore, the metallicity plays an essential role in stellar evolution and the amount of stellar mass loss (Langer et al. 1997, Charbonnel et al. 1999, Maeder & Meynet 2000ab, 2001, Dominguez et al. 2001b).

Specific nuclear physics features enter during the latest stages of stellar evolution. The high densities in late phases of O- and Si-burning result in partially or fully degenerate electrons with increasing Fermi energies (Nomoto & Hashimoto 1988). When these supercede the Q-value thresholds of electron capture reactions, this allows for electron capture on an increasing number of initially Si-group (sd-shell) and later Fe-group (pf-shell) nuclei. Because sd-shell reactions were well understood in the past (Fuller et al. 1985), O-burning predictions were quite reliable. The recent progress in calcu-

lating pf-shell rates (Langanke & Martinez-Pinedo 2000) led to drastic changes in the late phases of Si-burning (Heger et al. 2001ab).

Stars with masses $M>8M_\odot$ develop an onion-like composition structure, after passing through all hydrostatic burning stages, and produce a collapsing core at the end of their evolution, which proceeds to nuclear densities (Chieffi et al. 1998, Umeda et al. 2000, Heger et al. 2001ab). The recent change in electron capture rates sets new conditions for the Fe-core collapse after Si-burning, the size of the Fe-core and its electron fraction $Y_e=<Z/A>$ (Martinez-Pinedo et al. 2000) which are important ingredients for a type II supernova explosion.

Less massive stars experience core and shell H- and He-burning and end as C/O white dwarfs after strong episodes of mass loss (Hashimoto et al. 1993). Their ejected nucleosynthesis yields have initially been predicted by Renzini and Voli (1981). Recent reanalyses of their evolution and ejecta were undertaken by van den Hoek (1997) and Charbonnel et al. (1999). Shell He-burning is also identified as the source of the s-process, where $(\alpha$,n)-reactions, induced by the He-fuel, provide neutrons for sequences of neutron captures and beta-decays of unstable nuclei. ^{22}Ne(α,n) is a natural neutron source, with ^{22}Ne - originating from ^{14}N left over from H-burning - via ^{14}N$(\alpha,\gamma)^{18}$F$(e^+\nu_e)^{18}$O$(\alpha,\gamma)^{22}$Ne. Details of mixing processes play a role in providing the stronger neutron source ^{13}C(α,n), which requires the mixing of protons (hydrogen) into He-burning layers, leading to ^{12}C(p,$\gamma)^{13}$N $(e^+\nu_e)^{13}$C (Käppeler 1999, Busso et al. 2001, Van Eck et al. 2001).

More details about the production of heavy elements via slow and rapid neutron capture are given in section 6. Fig. 2 shows the decomposition of the solar abundances of heavy nuclei into the s- and r-process components (from Käppeler et al. 1989, Käppeler 1999).

Above, we discussed the "conventional" endstages of single star evolution with moderate progenitor masses, which dominate galactic nucleosynthesis. However, we know that above a (not yet well determined) limit in the range 25-60M$_\odot$ massive stars end with an Fe-core which is too large for a successful supernova explosion. This causes the central collapse to proceed to a stellar mass black hole. Dependent on a pending understanding of magneto-hydrodynamic effects, accretion of the remaining stellar envelope onto these black holes can lead to jets and "hypernova" explosions (MacFadyen & Woosley 1999, Cameron 2001ab, MacFadyen et al. 2001). The latter are possibly related to one class of gamma-ray bursts. Their nucleosynthesis has been discussed by Nakamura et al. (2001).

Very massive stars with several 100 M$_\odot$, which experience contraction due to the pair instability at high temperatures, undergo a complete disruption by explosive nuclear oxygen burning (VMOs, Heger & Woosley 2002). They should be considered in a similar way as hypernovae. The understanding of the initial mass function, describing the formation frequency as a function of progenitor mass, is, however, still marginal.

3 Type II Supernovae

The core collapse in massive stars, initiated via pressure reduction due to electron captures at the end of their stable evolution of hydrostatic core burning stages, leads to a bounce at nuclear densities and the formation of a hot neutron star which gained gravitational binding energy of the order 10^{53}erg (Bethe 1990). This provides neutrinos, diffusing out fast in comparison to other particles due to their small interaction cross sections. This was observed for SN 1987A (Burrows 1990). Neutrinos can deposit their energy via $\nu_e + n \rightarrow p + e^-$ and $\bar{\nu}_e + p \rightarrow n + e^+$ in adjacent layers. An energy deposition exceeding 10^{51}erg would be sufficient to cause an explosion and ejection of all layers surrounding the proto neutron star. The present situation in supernova modeling is that self-consistent spherically-symmetric calculations (with the presently known microphysics) do not yield successful explosions based on neutrino energy deposition from the hot collapsed central core (neutron star) into the adjacent layers (Rampp & Janka 2000). Even improvements in neutrino transport, solving the full Boltzmann transport equation for all neutrino flavors (Mezzacappa et al. 2001), and a fully general relativistic treatment (Liebendörfer et al. 2001ab, Liebendörfer et al. 2002) did not change this situation (see Figs.3 and 5). This seems to be the same for multi-D calculations (e.g. Mezzacappa et al. 1998), which however lack good neutrino transport schemes and do not yet consider the possible combined action of rotation and magnetic fields.

The hope that the neutrino driven explosion mechanism could still succeed is based on uncertainties which affect neutrino luminosities (neutrino opacities with nucleons and nuclei, Prakash et al. 2001), convection in the hot proto-neutron star (Keil & Janka 1995), as well as the efficiency of neutrino energy deposition (convection in the adjacent layers, Wilson & Mayle 1993). Fig. 4 shows the temporal Y_e and entropy evolution of the innermost zone of a 20 M$_\odot$ SN II simulation (Hauser et al. 2002), based on Liebendörfer et al. (2001a), but with varied neutrino opacities (reducing electron neutrino and antineutron scattering cross sections on nucleons by 60%) which permits a successful delayed explosion. This is only a parameter study, but it shows at least how options which increase the neutrino luminosity may lead to success.

Observations show typical kinetic energies of 10^{51} erg in supernova remnants. Thus, even without a correct understanding of the explosion mechanism, this permits one to perform light curve as well as explosive nucleosynthesis calculations by introducing a shock of appropriate energy in the pre-collapse stellar model (Woosley & Weaver 1986, Thielemann et al. 1990, Aufderheide et al. 1991, Woosley & Weaver 1995, Thielemann et al. 1996, Nomoto et al. 1997, Hoffman et al. 1999, Nakamura et al. 1999, Umeda et al. 2000, Rauscher et al. 2001a, 2002). Such induced calculations lack self-consistency and cannot predict the ejected ^{56}Ni-masses from the innermost explosive Si-burning layers (powering supernova light curves by the decay chain ^{56}Ni-^{56}Co-^{56}Fe) due to missing knowledge about the detailed explosion mechanism and therefore the mass cut between the neutron star and

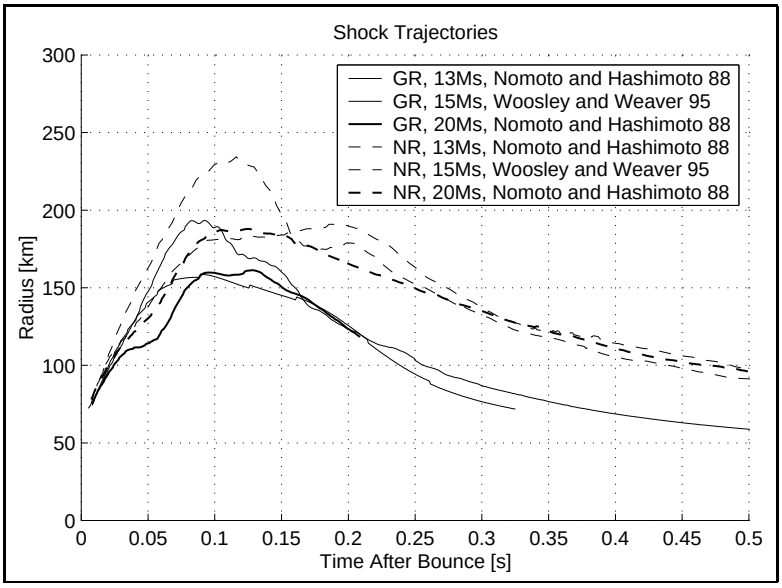

Fig. 3. Results of core collapse supernova simulations from Liebendörfer et al. (2002) for a variety of massive stellar models from Nomoto & Hashimoto (1988) and Woosley & Weaver (1995). Shown is the position of the shock as a function of time after central core bounce at nulear densities. We see that the shocks are strongest for the least massive stars. But all of them stall, recede and turn into accretion shocks, i.e. not causing successfull supernova explosions. For these (non-successful) simulations, the full general relativistic treatment (GR) weakens the shock further in comparison to the non-relativistic treatment (NR).

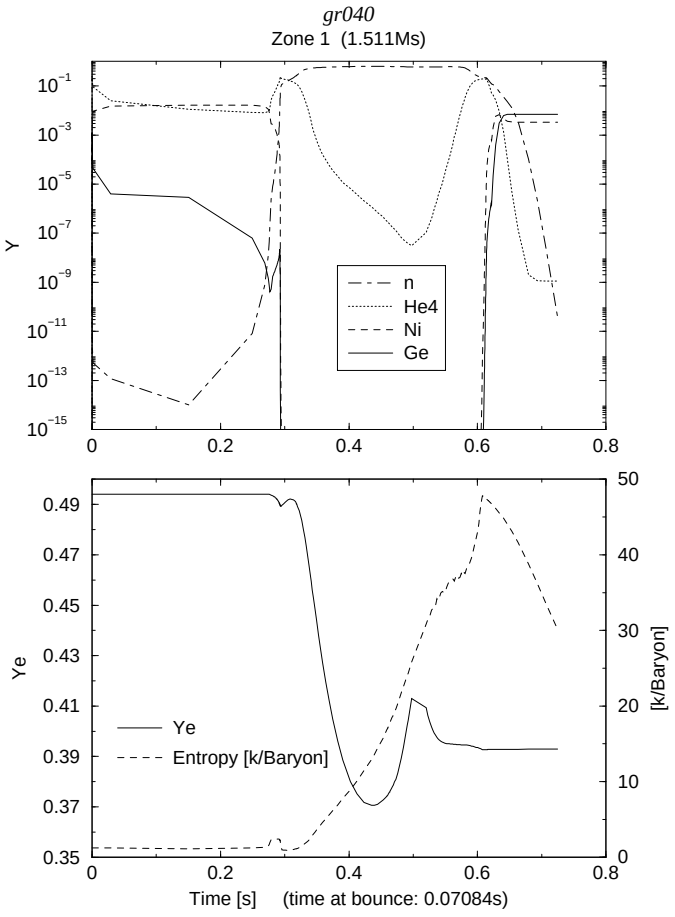

Fig. 4. Hydrodynamic simulations with varied (reduced) neutrino opacities (scattering cross sections on nucleons reduced by 60%) lead to larger neutrino luminosities and make successful supernova explosions possible (Hauser et al. 2002). Here we see the Y_e and entropy evolution of the innermost ejected zone of a 20$M_\odot$ star after core collapse, central bounce and neutrino heating (buttom). The top figure provides the composition evolution.

supernova ejecta. However, the intermediate mass elements Si-Ca are only dependent on the explosion energy and the stellar structure of the progenitor star, while abundances for elements like O and Mg are essentially determined by the stellar progenitor evolution. Thus, when moving in from the outermost to the innermost ejecta of a SN II explosion, we see an increase in the complexity of our understanding, depending (a) only on stellar evolution, (b) on stellar evolution and explosion energy, and (c) on stellar evolution and the complete explosion mechanism (see Fig. 6).

The possible complexity of the explosion mechanism, including multi-D effects, does not affect this (spherically symmetric) discussion of explosive nucleosynthesis severely. The 2D-calculations of Kifionidis et al. (2000) show a spherically symmetric shock front after the explosion is initiated, leading to spherical symmetry in explosive nuclear burning when passing through the stellar layers. Only after the passage of the shock front, the related temperature decline and freeze-out of nuclear reactions, the final nucleosynthesis products can be distributed in non-spherical geometries due to mixing by hydrodynamic instabilities. Thus, the total mass of nucleosynthesis yields shown in Fig. 6 is not changed, only its geometric distribution.

The correct prediction of the amount of Fe-group nuclei ejected (which includes also one of the so-called alpha elements, i.e. Ti) and their relative composition depends directly on the explosion mechanism and the size of the collapsing Fe-core. Three types of uncertainties are inherent in the Fe-group ejecta, related to (i) the total amount of Fe(group) nuclei ejected and the mass cut between neutron star and ejecta, mostly measured by ^{56}Ni decaying to ^{56}Fe, (ii) the total explosion energy which influences the entropy of the ejecta and with it the amount of radioactive ^{44}Ti as well as ^{48}Cr, the latter decaying later to ^{48}Ti and being responsible for elemental Ti, and (iii) finally the neutron richness or Y_e=$< Z/A >$ of the ejecta, dependent on stellar structure, electron captures

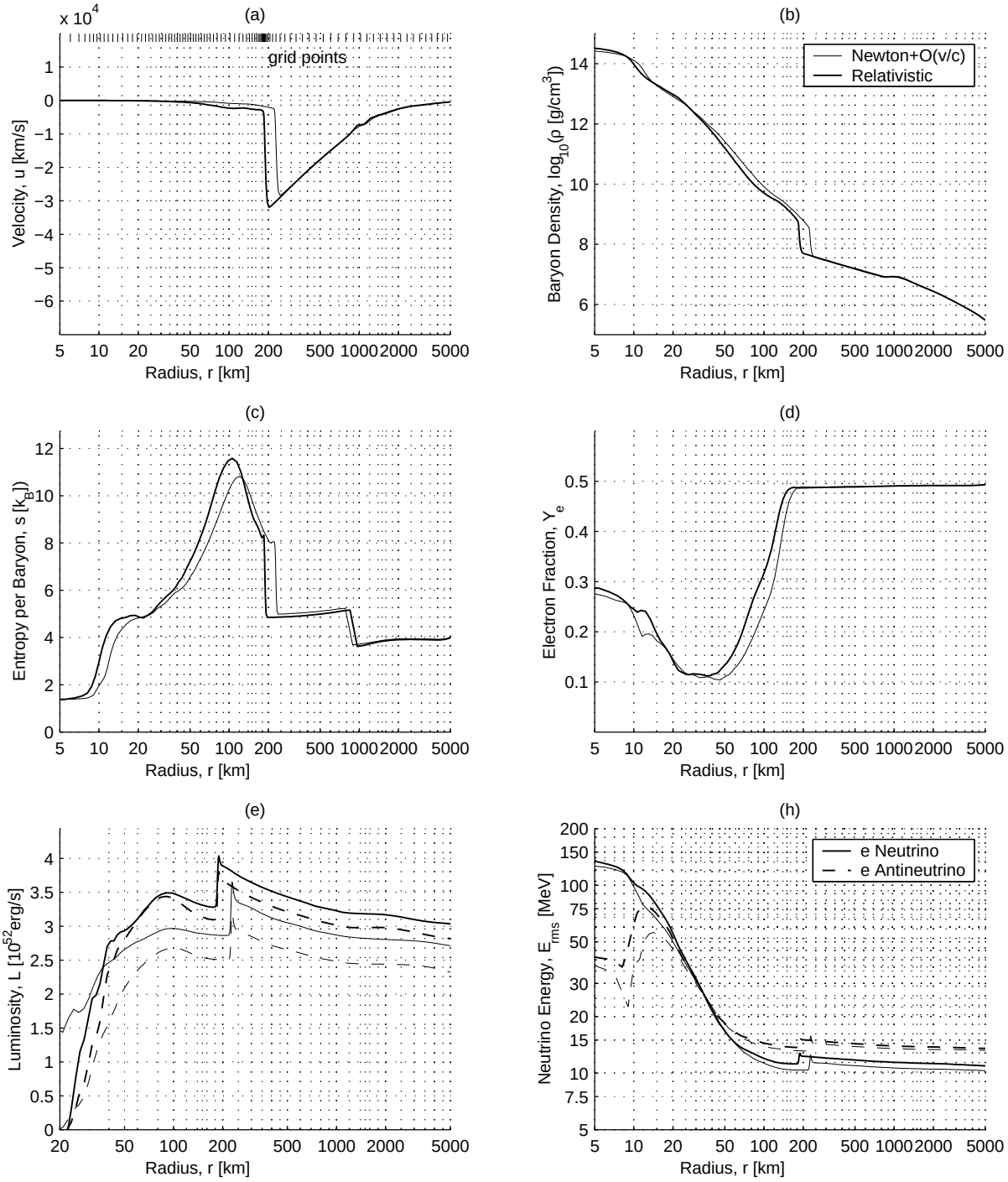

Fig. 5. Details from a core collapse and explosion simulation (Liebendörfer et al. 2001a) of a $13M_\odot$ stellar model from Nomoto & Hashimoto (1988) 100ms after the central bounce at nuclear densities in the phase of neutrino heating via $\nu_e + n \rightarrow p + e^-$ and $\bar{\nu}_e + p \rightarrow n + e^+$. A Newtonian hydro calculation with Boltzmann neutrino transport and terms up to the order v/c is compared to a fully general relativistic treatment in hydro and neutrino transport. Shown are (a) the velocity profile and the location of the adaptive grid points, (b) the rest mass density profile, (c) the entropy, (d) the electron fraction Y_e, the net electron (or proton) to nucleon ratio, i.e. a measure of the neutron-richness of matter, (e) the neutrino luminosity, and (f) the average energy of electron neutrinos and anti-neutrinos. We see that the shock is located at about 200km and at this point in time (100ms after bounce) has the features of an accretion shock (no positive velocities) rather than an outward moving shock. This underlines the negative outcome of spherically symmetric models with presently known microphysics.

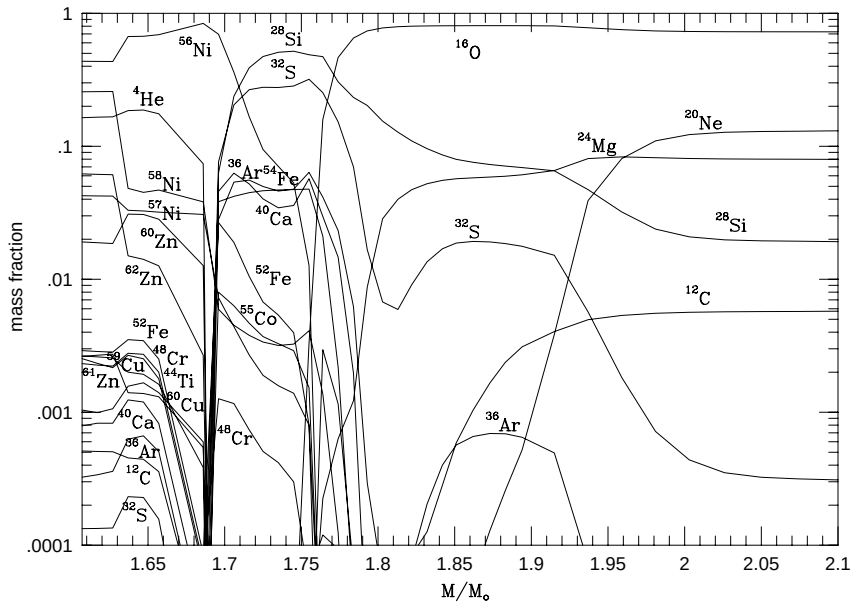

Fig. 6. Isotopic composition for the explosive C-, Ne-, O- and Si-burning layers of a core collapse supernova from a 20M$_\odot$ progenitor star with a 6M$_\odot$ He-core and an induced net explosion energy of 10^{51} erg, remaining in kinetic energy of the ejecta (from Thielemann et al. 1996). $M(r)$ indicates the radially enclosed mass, integrated from the stellar center. The exact mass cut in $M(r)$ between neutron star and ejecta and the entropy and Y_e in the innermost ejected layers depend on the details of the (still open) explosion mechanism. The abundances of O, Ne, Mg, Si, S, Ar, and Ca dominate strongly over Fe (decay product of ^{56}Ni), if the mass cut is adjusted to 0.07M$_\odot$ of ^{56}Ni ejecta as observed in SN 1987A.

and neutrino interactions. Y_e influences strongly the ratios of isotopes 57/56 in Ni(Co,Fe) and the overall elemental Ni/Fe ratio, the latter being dominated by ^{58}Ni and ^{56}Fe.

The pending understanding of the explosion mechanism also affects possible r-process yields for SNe II (Takahashi et al. 1994, Woosley et al. 1994, Qian & Woosley 1996, Freiburghaus et al. 1999a, McLaughlin et al. 1999, Nagataki & Kohri 2001, Thompson et al. 2001, Wanajo et al. 2001, Sumiyoshi et al. 2001). A more detailed discussion is given in section 6.

4 Type Ia Supernovae

There are strong observational and theoretical indications that SNe Ia are thermonuclear explosions of accreting white dwarfs in binary stellar systems (Höflich & Khokhlov 1996, Nugent et al. 1997, Nomoto et al. 2000, Livio 2001) with central carbon ignition leading to a thermonuclear runaway, because the pressure is dominated by a degenerate electron gas and shows no temperature dependence. This prevents a stable and controlled burning, causing a complete explosive disruption of the white dwarf (Nomoto et al. 1984, Woosley & Weaver 1994). The mass accretion rates determine the ignition densities. A flame front then propagates at a subsonic speed as a deflagration wave due to heat transport across the front (Hillebrandt & Niemeyer 2000).

The averaged spherical flame speed depends on the development of instabilities on various scales at the flame front. (The flame front thickness is of the order 10^{-4}cm and determined by heat conduction via the electron mean free path.) Multi-dimensional hydro simulations suggest a speed $v_{\rm def}$ as slow as a few percent of the sound speed $v_{\rm s}$ in the central region of the white dwarf. Electron capture affects the central electron fraction Y_e which depends on (i) the electron capture rates of nuclei, (ii) $v_{\rm def}$, influencing the time duration of matter at high temperatures (and with it the availability of free protons for electron captures), and (iii) the central density of the white dwarf ρ_{ign} (increasing the electron chemical potential i.e. the Fermi energy) (Iwamoto et al. 1999, Brachwitz et al. 2000, Langanke & Martinez-Pinedo 2000). After an initial deflagration in the central layers, the deflagration might turn into a detonation (supersonic burning front) at larger radii and lower densities (Niemeyer 1999). The nucleosynthesis consequences can be viewed in Fig. 7 (Brachwitz et al. 2002).

Nucleosynthesis constraints can help to find the "average" SN Ia conditions responsible for their contribution to galactic evolution, i.e. especially the Fe-group composition (Thielemann et al. 1986). Ignition densities ρ_{ign} dominate the very central amount of electron capture and thus Y_e. The deflagration speed $v_{\rm def}$ affects the time duration of burning in a zone and with it the possible amount of electron captures on free protons and nuclei. It is also responsible for the time delay between the arrival of the information that a burning front is approaching (the information is propagating with sound

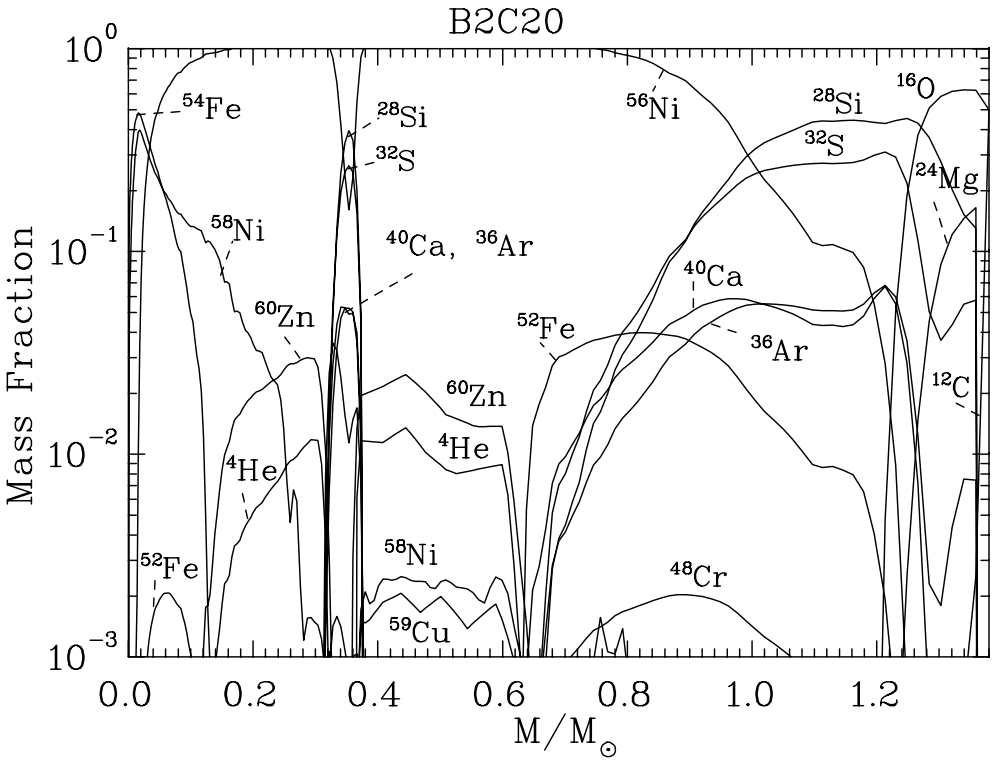

Fig. 7. Isotopic composition for the layers of a type Ia supernova, starting thermonuclear burning with a deflagration front which turns into a detonation at 0.32 $M_\odot$. This is shown in the ^{56}Ni feature which sandwiches explosive O-burning products like ^{28}Si through ^{40}Ca. $M(r)$ indicates the radially enclosed mass, integrated from the stellar center. We see the products of explosive Si-burning (^{56}Ni), O-burning (^{28}Si), Ne-burning (^{16}O and ^{24}Mg), minor amounts of C-burning (^{20}Ne) and unburned matter at the surface. The central Fe-group composition depends on Y_e which is directly related to the amount of electron capture on free protons and nuclei.

speed and causes expansion of the outer layers) and the actual arrival of the burning front. Burning at lower densities causes less electron captures. Thus, $v_{\rm def}$ determines the resulting Y_e -gradient as a function of radius (Iwamoto et al. 1999). Y_e values of 0.47-0.485 lead to dominant abundances of ^{54}Fe and ^{58}Ni, values between 0.46 and 0.47 produce dominantly ^{56}Fe, values in the range of 0.45 and below are responsible for ^{58}Fe, ^{54}Cr, ^{50}Ti, ^{64}Ni, and values below 0.43-0.42 are responsible for ^{48}Ca. The intermediate Y_e-values 0.47-0.485 exist in all cases, but the masses encountered which experience these conditions depend on the Y_e-gradient and thus v_{def}. Whether the lower values with Y_e<0.45 are attained, depends on the central ignition density ρ_{ign}. Therefore, ^{54}Fe and ^{58}Ni are indicators of v_{def} while ^{58}Fe, ^{54}Cr, ^{50}Ti, ^{64}Ni, and ^{48}Ca are a measure of ρ_{ign}. A test for these (hydrodynamic) model parameters is shown in Fig. 8 where B1 and B2 indicate increasing propagation speeds of the burning front and C20 through C80 increasing ignition densities (results from Brachwitz et al. 2002).

Nuclear uncertainties based on electron capture rates enter as well (Brachwitz et al. 2000, 2002). Conclusions from these results are: (i) a v_{def} in the range 1.5–3% of the sound speed is preferred (Iwamoto et al. 1999), and (ii) the change in electron capture rates (Langanke & Martinez-Pinedo 2000) made it possible to have ignition densities as high as ρ_{ign}=2$\times$ 10^9 g cm^{-3} (as expexted from typical accretion rates, see e.g.

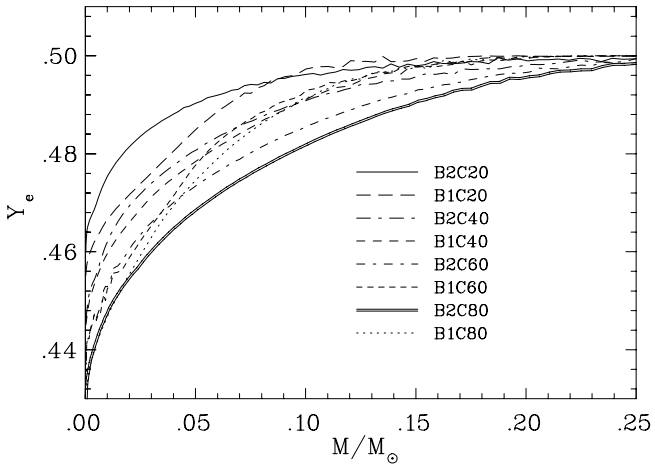

Fig. 8. Y_e after freeze-out of nuclear reactions measures the electron captures on free protons and nuclei. Small burning front velocities lead to steep Y_e-gradients which flatten with increasing velocities (see the series of B1 vs. the B2 models). Lower central ignition densities shift the curves up (see changes from C20 through C80, i.e. central ignitions at 2-8$\times$10^9 g cm^{-3}), but the gradient is the same for the same propagation speed (from Brachwitz et al. 2002).

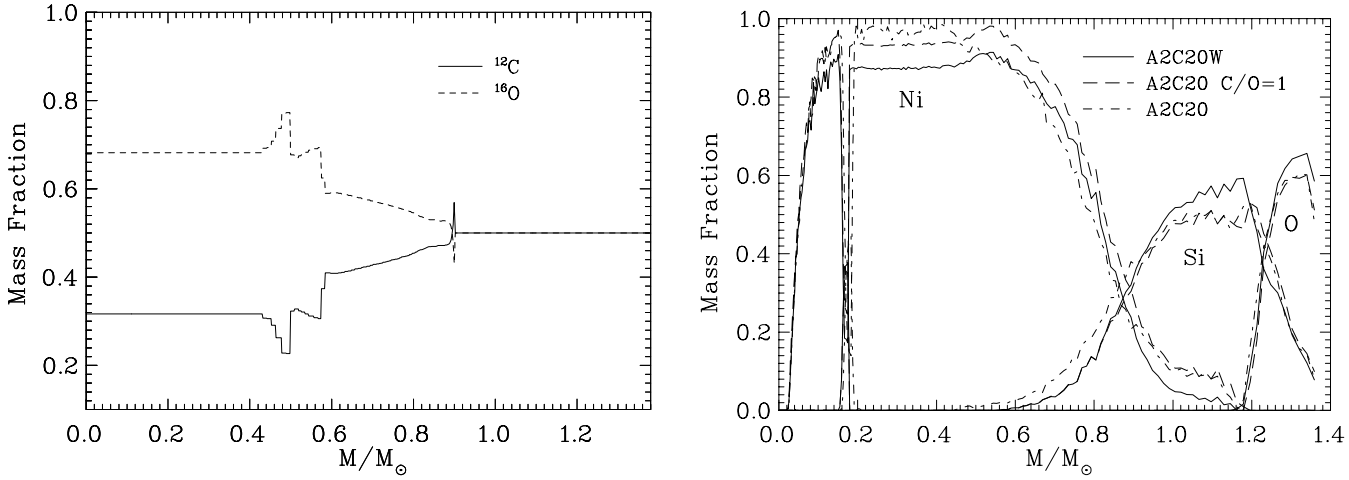

Fig. 9. Left: Mass fractions of C and O throughout the white dwarf before undergoing thermonuclear ignition. The inner part (where O dominates) shows the initial white dwarf before accretion, the outer part the matter which underwent H- and He-burning during the accretion phase (at higher temperatures) where the mass fractions of C and O are comparable. Right: Mass fractions of Ni (^{56}Ni), Si (^{28}Si) and O (^{16}O) throughout the white dwarf after a thermonuclear explosion. The model A2C20 stands for a burning front propagation of 2% of the sound speed and a central ignition density of 2×10^9 g cm^{-3} and is based on a white dwarf composition as indicated on the left. C/O=1 stands for a modified white dwarf composition with equal amounts of C and O also in the inner region of the original white dwarf. The third model A2C20W reflects a higher metallicity of the material. This is measured by the amount of ^{22}Ne (2.5% in comparison to 1% for the other models, Brachwitz et al. 2002).

Dominguez et al. 2001a) without destroying the agreement with solar abundances of very neutron-rich species (Brachwitz et al. 2000). It seems, however, hard to produce amounts of ^{48}Ca sufficient to explain solar abundances from SNe Ia (in spherical symmetry) when applying more realistic electron capture rates, even for very high ignition densities (Woosley 1997, Brachwitz et al. 2002).

While uncertainties in the detailed 3D burning front propagation have been parametrized in terms of propagation speed and detonation transition density, it is expected that in a self-consistant simulation both "parameters" will adjust themselves to unique values for the same initial models. The ignition density is a system indicator, reflecting the accretion history in a binary system. A similar hidden system parameter is the mass of the initial white dwarf, which determines the C/O ratio within the original white dwarf before accretion sets in (Höflich 2000, Dominguez et al. 2001a and Fig. 9 left). The accretion burning at higher temperatures leads always to comparable C and O mass fractions.

Fig. 9 (right) shows the resulting abundances for explosions with different C/O ratios also in the central part of the initial white dwarf (C and O like in Fig. 9 left or C/O=1). The reason is related to the different energy release for burning ^{16}O or ^{12}C to ^{56}Ni. A further change is seen if the metallicity of the object (or the accreted matter) is changed. Existing CNO burns in H-burning to ^{14}N and in He-burning to ^{22}Ne, a nucleus with two more neutrons than protons. This affects the energy generation in the outer Si-burning layers, where the neutron-richness of matter is not due to electron captures as in the inner high-density layers but originating from the initial pre-ignition composition (measured here in the fraction of ^{22}Ne, 1 vs. 2.5% in case W). We see how the production of ^{56}Ni is changed which directly determines the light curve properties. The central C/O ratio, reflecting the white dwarf mass in the pre-explosion binary system (Domiguez et al. 2001a), can thus serve as a parameter which determines the supernova and lightcurve properties and must be related to the empiricial brightness/decline relation (Riess et al. 2000, Leibundgut 2001). In Fig. 9 we see, however, also that the initial metallicity (measured by the original ^{22}Ne content) can have similar effects. This introduces an empirical two rather than one parameter dependence (see also Höflich et al. 1998). However, detailed analyses by Dominguez et al. (2001a) have shown that the latter effect is smaller than the observational changes towards high redshifts. This supports the cosmological use of SNe Ia also at high redshifts.

The general nucleosynthesis outcome of SNe Ia is dominated by Fe-group products, but involves sizable fractions of Si-Ca and minor amounts of unburned or pure C-burning products (e.g. C, O, Ne, Mg). The ratio of Fe to Si-Ca is about a factor of 2-3 higher than in solar composition (Grevesse & Sauval 1998). This typical feature is shown in Fig. 10 for models discussed above. In principle one expects major differences for the Fe-group composition as a function of parameters like burning front propagation and ignition density (Iwamoto et al. 1999, Brachwitz et al. 2000). Here we present models which agree with the general constraints but also show a change in metallicity. One difference which becomes apparent immediately is the change in Mn. ^{55}Mn (the only stable isotope of Mn) is a decay product of ^{55}Co which is mainly produced in incomplete Si-burning. In this respect it was discussed by Iwamoto et al. (1999) as an indicator of the deflagration-detonation transition in delayed detonation

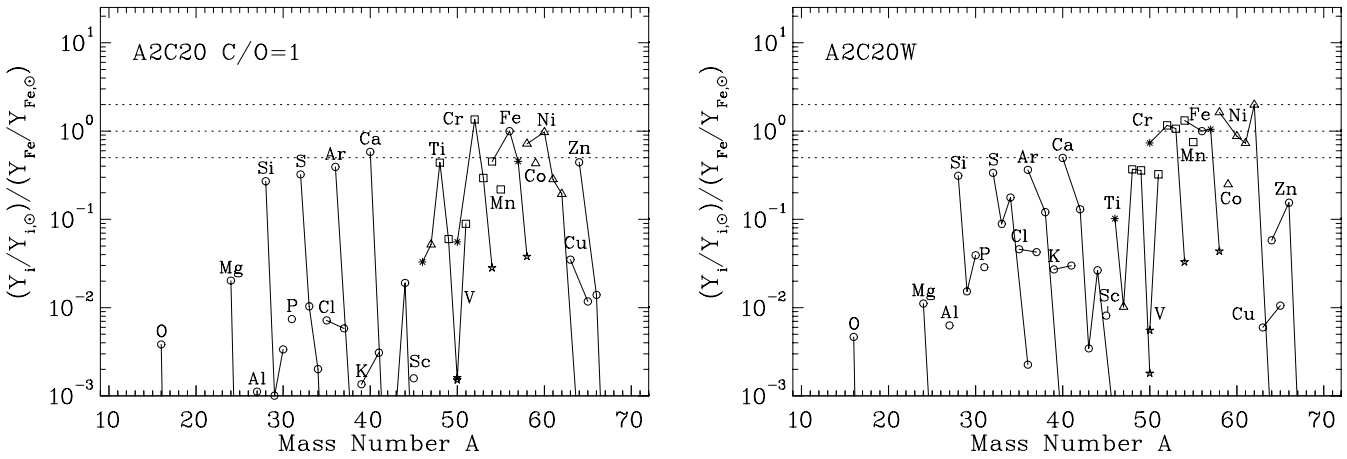

Fig. 10. Abundance ratios of nuclei compared to their solar values and normalized for ^{56}Fe, the decay product of ^{56}Ni. Isotopes of the same element are connected by lines. The general feature is that the ratio of Fe to Si-Ca is about a factor of 2-3 higher than solar. For the changes in the Fe-group composition see text (from Brachwitz et al. 2002).

models. Here we see that it is affected by metallicity as well (strongly changing from A2C20 to A2C20W, more details in Brachwitz et al. 2002).

5 Novae and X-ray Bursts

5.1 Novae and explosive hydrogen burning

The major astrophysical events which involve explosive H-burning are novae and type I X-ray bursts. Both are related to binary stellar systems with hydrogen accretion from a binary companion onto a compact object at small accretion rates which leave the H/He-fuel unburned. In the case of novae the compact object is a white dwarf, in the case of X-ray bursts it is a neutron star. Ignition sets in when a critical layer mass ΔM is surpassed, in novae (dependent on the white dwarf mass) of the order $10^{-5} - 10^{-4}$M$_\odot$, in type I X-ray bursts of the order 10^{-9}M$_\odot$. This leads to explosive ignition of the accreted H-layer under degenerate conditions (similar to central C-ignition in SNe Ia). For high densities the pressure is dominated by the degenerate electron gas and shows no temperature dependence. This prevents a stable and controlled burning, leading therefore to a thermonuclear runaway. While the ignition is always based on pp-reactions (as in solar hydrogen burning), the runaway leads to the hot CNO-cycle ^{12}C(p,γ)^{13}N(p,γ)^{14}O($e^+\nu$)^{14}N(p,γ)^{15}O($e^+\nu$) ^{15}N(p,α) ^{12}C, branching out partially via ^{15}N(p,γ)^{16}O(p,γ) ^{17}F($e^+\nu$) ^{17}O(p,γ)^{18}F...

In essentially all nuclei below Ca, a proton capture reaction on the nucleus (Z_{even}–1,N=Z_{even}) produces the compound nucleus above the alpha-particle threshold and permits a (p,α) reaction. This is typically not the case for (Z_{even}–1,N=Z_{even}–1) due to the smaller proton separation energy and leads to hot CNO-type cycles above Ne (Thielemann et al. 1994, see Fig. 11). There is one exception, Z_{even}=10, where the reaction ^{18}F(p,α) is possible, avoiding ^{19}F and a possible leak via ^{19}F(p,γ) into the NeNaMg-cycle. This has

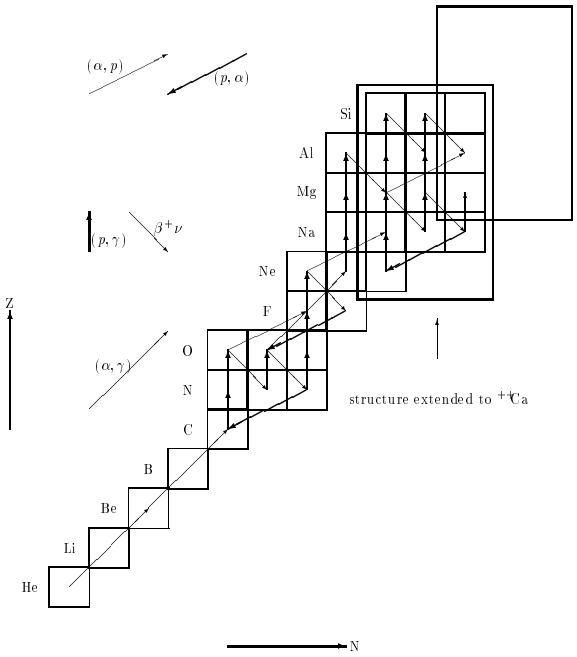

Fig. 11. The hot CNO-cycle incorporates three proton captures, (^{12}C, ^{13}N, ^{14}N), two β^+-decays (^{14,15}O) and one (p, α)-reaction (^{15}N). In a steady flow of reactions the long beta-decay half-lives are responsible for high abundances of ^{15,14}N (from ^{15,14}O decay) in nova ejecta. From Ne to Ca, cycles similar to the hot CNO exist, based always on alpha-nuclei like ^{20}Ne, ^{24}Mg etc. The exception is the (not completed) cycle based on ^{16}O, due to ^{18}F(p,α)^{15}O, which provides a reaction path back into the hot CNO-cycle. Thus, in order to proceed from C to heavier nuclei, alpha-induced CNO breakouts are required. The shown flow pattern, which includes alpha-induced reactions, applies for temperatures in the range 4-8$\times 10^8$ K. Smaller temperatures permit already processing of pre-existing Ne via hot CNO-type cycles. This leads to the typical nova abundance pattern with ^{15,14}N enhancements, combined with specific isotopes up to about Si or even Ca. If the white dwarf is an ONeMg rather than CO white dwarf, containing Ne and Mg in its initial composition resulting from carbon rather than helium burning, the latter feature is specifically recognizable.

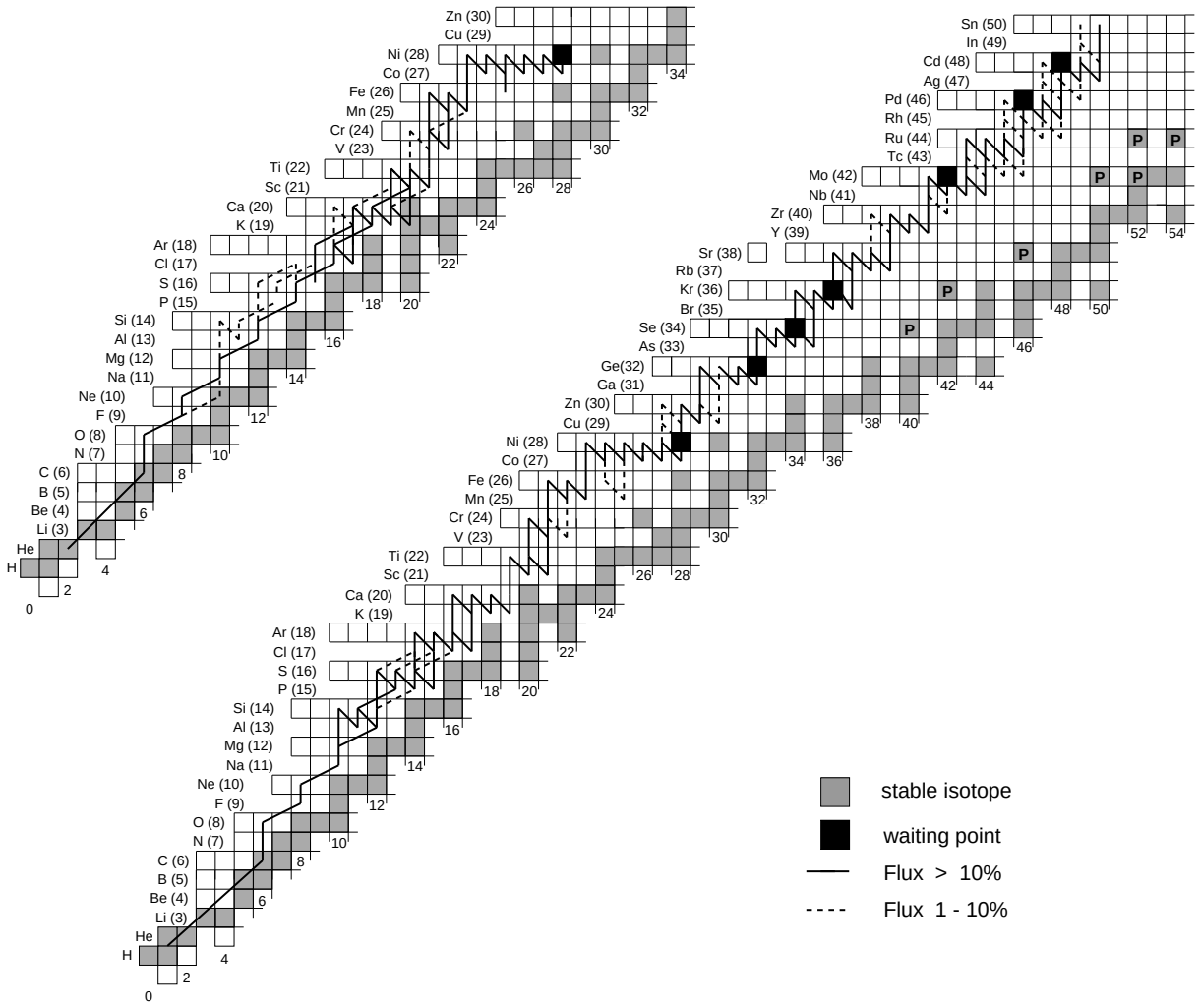

Fig. 12. rp and αp-process flows up to and beyond Ni. The reaction flows shown in the nuclear chart are integrated reaction fluxes from a time dependent network calculation (Wiescher & Schatz 2000), (a) during the initial burst and thermal runaway phase of about 10s (top left), (b) after the onset of the cooling phase when the proton capture on ^{56}Ni is not blocked anymore by photodisintegrations (extending for about 200s, bottom right). Waiting points above ^{56}Ni are represented by filled squares, stable nuclei by hatched squares, light p-process nuclei below A=100 are indicated by a P.

the effect that only alpha induced reactions like ^{15}O(α,γ) can aid a break-out from the hot CNO-cycle to heavier nuclei beyond Ne (Wiescher et al. 1999). Break-out reactions from the hot CNO-type cycles above Ne proceed typically via proton captures on the nucleus (Z_{even},N=Z_{even}-1) and permits a faster build-up of heavier nuclei (Thielemann et al. 1994, Rembges et al. 1997). They occur at temperatures of about 3×10^8K, while the alpha-induced break-out from the hot CNO-cycle itself is delayed to about 4×10^8K.

Explosive H-burning in novae has been discussed in many recent articles (José et al. 1999, Starrfield 1999, Starrfield et al. 2000, Coc et al. 2000, José et al. 2001). Its processing seems limited due to maximum temperatures of $\sim$3$\times10^8$K. Apparently, only in X-ray bursts temperatures larger than 4×10^8K are possible. This is important, because it leads to a quite different outcome of hot/explosive H-burning. The major nucleosynthesis yields for novae are therefore related to hot CNO-products like ^{15}N and specific nuclei between Ne and Si/S, which are based on processing of pre-existing Ne (more details are discussed together with Fig. 11).

5.2 Type I X-ray bursts

In type I X-ray bursts (Taam 1985, Lewin et al. 1993, Taam et al. 1996, Schatz H. et al. 1998, 2001, Wiescher & Schatz 2000) hydrogen, and subsequently also helium, burn explosively in a thermonuclear runaway. Once the hot CNO-cycle, and hot CNO-type cycles beyond Ne, have generated sufficient amounts of energy in order to surpass temperatures of $\sim4\times10^8$K, alpha-induced reactions lead to a break-out from the hot CNO-cycle. This provides new fuel for reactions beyond Ne, leading to a further increase in temperature.

In the next stage of the ignition process also He is burned via the 3α-reaction ^{4}He$(2\alpha,\gamma)^{12}$C, filling the CNO reservoir, and the αp-process (a sequence of (α,p) and (p,γ) re-

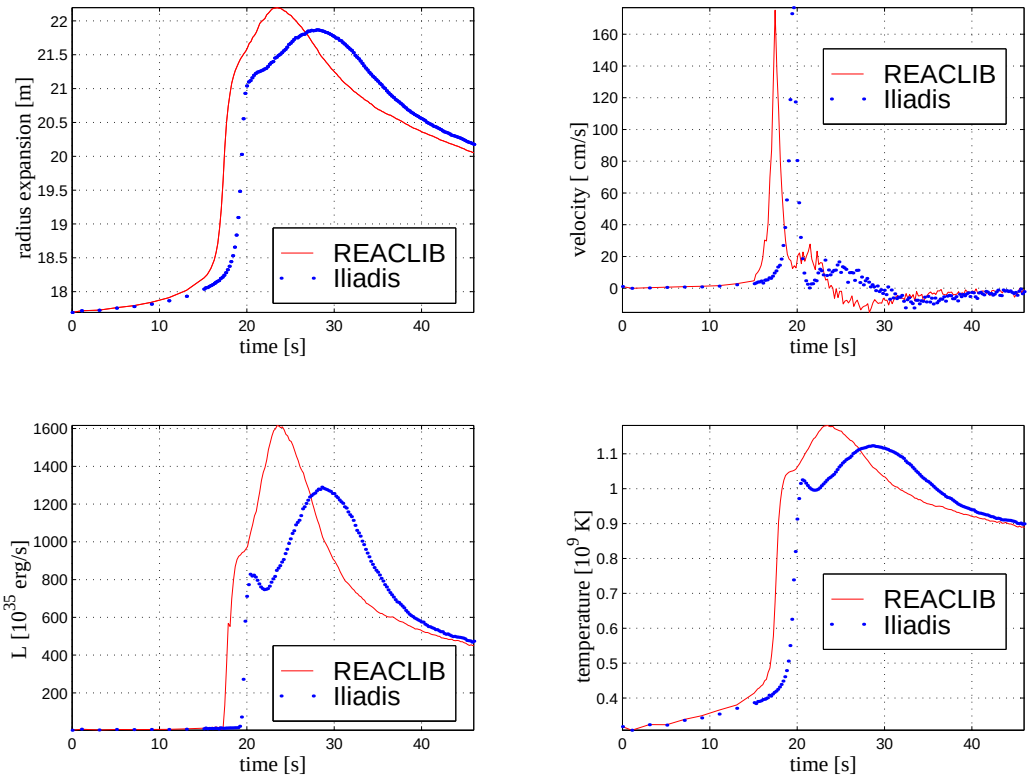

Fig. 13. Comparison of burst profiles with different proton capture rates for the break-out reactions on ^{27}Si, ^{31}S, ^{35}Ar, and ^{38}Ca in a self-consistent X-ray burst model (Rembges 1999, Rauscher et al. 2000). Due to different reaction rates, matter beyond Ne is burned on different timescales, causing a different pre-expansion before the maximum temperature is attained during alpha-induced reaction sequences.

actions, Wallace & Woosley 1981) sets in. It produces nuclei up to Ca and provides seed nuclei for hydrogen burning via the rp-process (proton captures and beta-decays). Processing of the αp-process and rp-process up to and beyond ^{56}Ni is shown in Fig. 12 (Wiescher & Schatz 2000). Certain nuclei play the role of long waiting points in the reaction flux, where long beta-decay half-lives dominate the flow, either competing with slow (α,p) reactions or negligible (p,γ) reactions, because they are inhibited by inverse photodisintegrations for the given temperatures. Such nuclei were identified as ^{25}Si ($\tau_{1/2}$=0.22s), ^{29}S (0.187s), ^{34}Ar (0.844s), ^{38}Ca (0.439s). The bottle neck at ^{56}Ni can only be bridged for minimum temperatures around 10^9K (in order to overcome the Coulomb barrier for proton capture) and maximum temperatures below 2×10^9K (in order to avoid photodisintegrations), combined with high densities exceeding 10^6g cm^{-3} which support the capture process (Schatz et al. 1998, Rehm et al. 1998). If this bottle neck can be overcome, other waiting points like ^{64}Ge (64s), ^{68}Se (96s), ^{74}Kr (17s) seem to be hard to pass. However, partially temperature dependent half-lives (due to excited state population), or mostly 2p-capture reactions via an intermediate proton-unstable nucleus (introduced in Görres et al. 1995 and applied in Schatz et al. 1998) can help. The final endpoint of the rp-process was found recently by Schatz et al. (2001), who determined a closed reaction cycle in the Sn-Sb-Te region, due to increasing alpha-instability of heavy proton-rich nuclei.

The initial break-out reactions from hot CNO-type cycles and the hold-ups at waiting points introduce a time structure in energy generation. One of the essential questions is whether they can/will show up in the X-ray light-curves of bursts. The other question is whether individual proton-capture reactions matter, because at peak temperatures (p,γ)-(γ,p) equilibria are attained, determined only by nuclear masses of the nuclei involved. This leads to a chemical equilibrium distribution for proton-capture reactions along isotonic lines and a steady flow of beta-decays between these equilibrium abundance maxima. Therefore, Iliadis et al. (1999) claimed that individual (p,γ)-reactions do not influence burst properties, based on nucleosynthesis calculations utilizing an X-ray burst temperature profile provided by Rembges (1999). This paper showed (as should be expected from the final equilibrium conditions) that, with a given temporal temperature profile, the resulting composition does not depend on individual reactions. The important question, however, is whether the feedback from hydrodynamics, due to the changed energy input in the early ignition stages during the working of break-out reactions, leads to different temperature profiles and thus different final abundances.

The results of a self-consistent calculation can be seen in

Fig. 13 from (Rembges 1999, Rauscher et al. 2000), which shows the radius of the burning shell, the velocity, the luminosity, and the temperature. The difference between calculations with the old REACLIB rates (Thielemann et al. 1987, Cowan et al. 1991) and the ones with updated cross sections for the break-out points ^{27}Si, ^{31}S, ^{35}Ar, and ^{38}Ca emerges at the expected temperatures of $(3-4)\times10^8$K, when these break-out reactions occur. At that point the nuclei beyond Ne will burn towards Ni/Fe. This energy input causes the temperature increase which will at first permit the hot CNO break-out via alpha-induced reactions, followed by the triple-alpha link to ^{12}C. This leads to the burning of ^{4}He and determines the temperature peak of the rp-process with a chemical equilibrium for proton-capture reactions. However, as the initial break-out phase differs, different pre-expansions can occur, causing different densities and also different peak temperatures.

This effect was recently underlined in further self-consistent burst calculations (Fisker et al. 2001b, Wiescher et al. 2002), when REACLIB rates in the mass range A=44–63 were replaced by cross sections based on resonance properties from shell model calculations (Fisker et al. 2001a). These effects are even more drastic, again due to the early burning phase when matter beyond Ne burns up to Fe, before the alpha-captures begin. This shows that a more precise determination of specific reaction rates is important, when self-consistent network plus hydrodynamics calculations are performed. The peak temperatures and densities attained in X-ray burst calculations depend on this cross sections input. They depend, however, also on a correct modeling of the deeper neutron star crust layers, which consist of ashes of previous bursts. Electron captures due to higher densities in deeper layers and ignition of previously unburned ashes can lead to higher temperatures at the inner boundaries of the unburned H/He-layer and even cause so-called "superbursts" (Cummings & Bildsten 2001). Thus, it is paramount not just to model the H/He-layers with inner boundary conditions (Rembges 1999, Rauscher et al. 2000, Fisker et al. 2001b, Wiescher et al. 2002), but to model consistently the deeper layers as well.

If only a small percentage of the synthesized matter in X-ray bursts escapes the strong gravitational field of the neutron star, some proton-rich stable nuclei (p-process nuclei) below A=100 (indicated as P in Fig. 12) could be explained in the solar system abundances. The more massive p-process isotopes (contributing only 1% or less to their element abundances) are probably due to $(\gamma$,n) and (γ,α) "spallation" reactions of pre-existing stable nuclei during explosive burning in those mass zones of supernovae which attain temperatures of about 2×10^9K (Woosley & Howard 1978, Costa et al. 2000, Rauscher et al. 2001b, Rauscher et al. 2002).

6 Heavy Elements: r- and s-Process

6.1 Neutron capture processes

It is long understood that the existence of the heavy elements in nature is due to neutron capture (Suess & Urey 1956) and that (at least) two types of processes must be responsible (Burbidge et al. 1957, Cameron 1957): 1. A process with small neutron densities, experiencing long neutron capture timescales in comparison to β-decays ($\tau_\beta < \tau_{n,\gamma}$, slow neutron capture or the s-process), causing abundance peaks in the flow path at nuclei with small neutron capture cross sections. These are stable nuclei with closed shells, i.e. magic neutron numbers (Käppeler et al. 1989). 2. A process with high neutron densities and temperatures, experiencing rapid neutron captures and the reverse photodisintegrations with $\tau_{n,\gamma},\tau_{\gamma,n} < \tau_\beta$. This leads to chemical equilibria for neutron captures along isotopic chains and the rapid neutron-capture process (r-process) produces highly unstable nuclei with short half-lives (Kratz et al. 1993, Käppeler et al. 1998, Pfeiffer et al. 2001), permitting also the formation of the heaviest elements in nature like Th, U, and Pu. The r-process involves nuclei near the neutron drip-line, where the last neutron is not bound and thus the neutron binding or neutron separation energy is zero or negative. Far from stability, neutron shell closures are encountered for smaller mass numbers than in the valley of stability. Therefore, a steady flow of beta-decays between the maxima of isotopic equilibrium chains causes r-process peaks due to long β-decay half-lives. These are encountered closest to stability at neutron-magic nuclei. Therefore, the r-process abundance peaks are shifted in comparison to the s-process peaks (which occur for neutron shell closures at the stability line).

This behavior is indicated in Fig. 14. The r-process runs along equilibrium maxima at constant neutron separation energy. One such line with S_n=3.3MeV is shown in the nuclear chart. The peaks are given by the longest beta-decay half-lives (closest to stability at shell closures). After decay, this results in an abundance distribution as a function of mass number A as shown in the inserted graph. The s-process maxima occur for the smallest neutron capture cross sections at closed shells (magic numbers) along the line of stability. Therefore, the r-process peaks are shifted to lower mass numbers. The decomposition of solar abundances of heavy nuclei into s- and r-process components has been shown in Fig. 2 and presented with a basic discussion of the s-process and its sites. Here we want to concentrate on the r-process.

Besides this basic understanding, the history of r-process research has been quite diverse in suggested scenarios (for reviews see Cowan et al. 1991, Wallerstein et al. 1997, Käppeler et al. 1998, Pfeiffer et al. 2001). If starting with a seed distribution somewhere around A=50-80, before rapid neutron-capture sets in, the operation of an r-process requires 10 to 150 neutrons per seed nucleus to form all heavier r-nuclei. The question is which kind of environment can provide such a supply of neutrons which need to be utilized before decaying with a 10 min half-life. The logical conclusion is that only explosive environments, producing or releasing these neutrons suddenly, can account for such conditions. Two as-

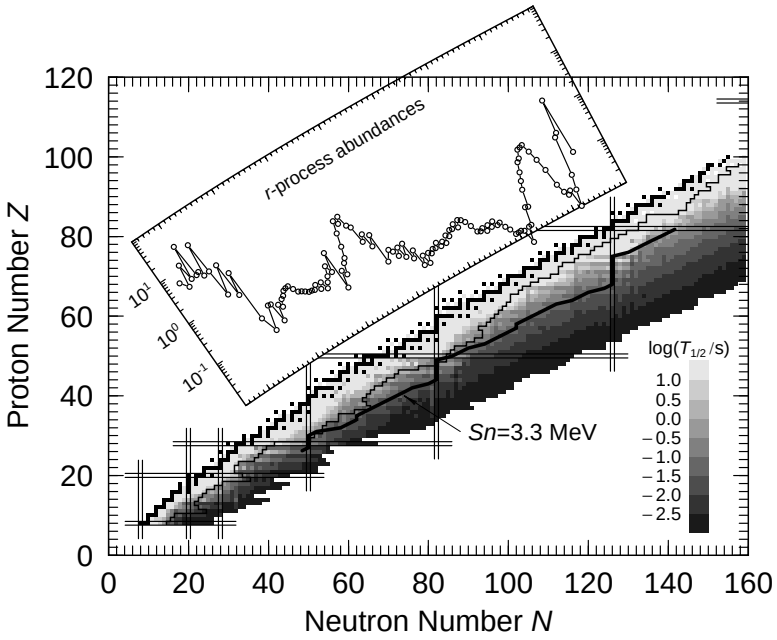

Fig. 14. Some features of nuclei in the (N, Z)-chart of isotopes. Stable nuclei are indicated by black filled squares. The thin solid line represents the present limit of experimentally known nuclear masses. The magic numbers are shown as double bars. The thick solid line is the contour line of constant neutron separation energy S_n=3.3 MeV. It relates nuclear properties to astrophysical abundances of the r-process. It can be recognized that the abundances are proportional to the β^--decay half-lives [indicated by grey shades in $\log_{10}(\tau_{1/2})$] along S_n contour lines.

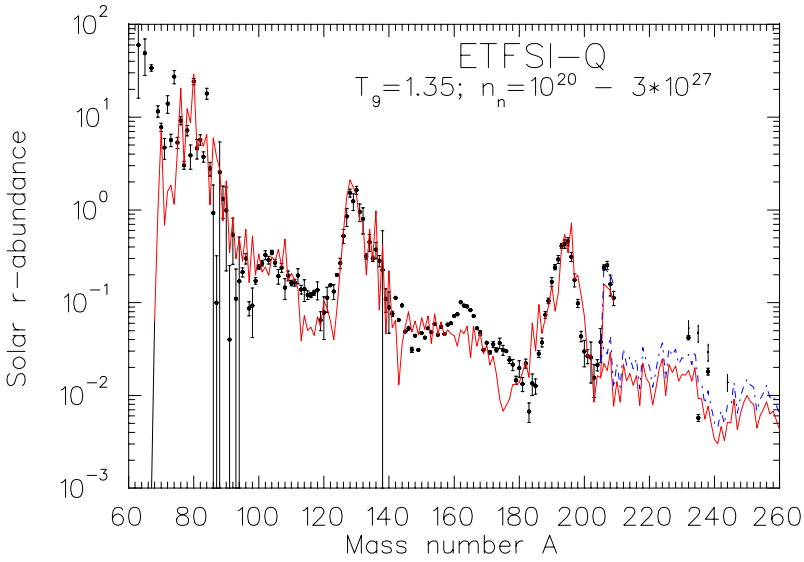

Fig. 15. Fits to solar r-process abundances, obtained with two different smooth superposition of 17 equidistant $S_n(n_n, T)$ components from 1 to 4 MeV (solid and dashed lines). The ETFSI-Q mass model (Pearson et al. 1996) was applied, which introduces a phenomenological quenching of shell effects. The quenching of the $N = 82$ shell gap avoids a large abundance trough below the A=130 peak. These results also show a good fit to the r-process Pb and Bi contributions after following the decay chains of unstable heavier nuclei (indicated by two sets - dashed lines - of abundances for A>205).

trophysical settings are suggested most frequently: (i) Type II supernovae with postulated high-entropy ejecta (Woosley et al. 1994, Takahashi et al. 1994, Qian & Woosley 1996, Meyer et al. 1998, Otsuki et al. 2000, Freiburghaus et al. 1999a, Nagataki & Kohri 2001, Wanajo et al. 2001, Thompson et al. 2001) and (ii) neutron star mergers or similar events (like axial jets in supernova explosions) which eject neutron star matter with low-entropies (Lattimer et al. 1977, Meyer 1989, Eichler et al. 1989, Freiburghaus et al 1999b, Rosswog et al. 1999, 2000, 2001, Cameron 2001ab). These two sites are representative for two (high or low) entropy options.

6.2 Working of the r-process and solar r-abundances

First, we want to discuss here some general features. The high neutron density and temperature environments, leading to an r-process, result in a chemical equilibrium for neutron captures and the reverse photodisintegrations $(n, \gamma) \rightleftharpoons (\gamma, n)$ within isotopic chains for each element and cause abundance maxima at a specific neutron separation energy. Thus, the combination of a neutron density n_n and temperature T determines the r-process path defined by a unique neutron separation energy S_n. Therefore a choice of either (n_n, T) or S_n for an r-process is equivalent. During an r-process event exotic nuclei with neutron separation energies of 4 MeV and less are important, up to S_n=0, i.e. the neutron drip-line. This underlines that the understanding of nuclear physics far from stability is a key ingredient (Kratz et al. 1998).

Traditionally, before having knowledge of a particular r-process model (site), attempts were made to fit solar r-process abundances with a choice of neutron number densities n_n, temperatures T and exposure timescales τ. Our r-process parameter studies showed that the entire isotopic abundance pattern cannot be reproduced by assuming a unique r-process path, characterized by one neutron separation energy (Thielemann et al. 1993, Kratz et al. 1993). Instead, even in a single

astrophysical event it requires a superposition of a multitude of r-components (a minimum of three) with different neutron densities or equivalently different S_n's, related to different r-process paths and time scales (Chen et al. 1995, Goriely & Arnould 1996, Cowan et al. 1999, Freiburghaus et al. 1999a). In Fig. 15 we show global abundance distributions from a superpostion of sixteen n_n, T, τ components, utilizing the ETFSI-Q (Pearson et al. 1996) nuclear mass model. The successful reproduction of the position and relative height of the peaks, as well as the remaining deficiencies, have been interpreted as signatures of nuclear structure near the neutron drip-line (Thielemann et al. 1994, Chen et al. 1995, Kratz et al. 1998, Kratz et al. 2000, Pfeiffer et al. 2001).

A more realistic astrophysical setting is given by an explosion (leading to initial entropies) and adiabatic expansion (Hoffman et al. 1996, 1997). In a superposition of high-entropy environments, the high entropies (up to 400 k_b/nucleon, responsible for the mass region A>110) reproduce nicely the r-abundance pattern. Some exceptions in the mass region 110–120 are related - as in the site-independent studies with n_n, T, τ - to nuclear structure effects at the shell closures N=82. Thus, both approaches can have a nearly one-to-one mapping between their resulting abundance features (Freiburghaus et al. 1999a). Discrepancies occur in the mass region 80–110, for which lower entropies are responsible. The reason is that essentially no neutrons are left after the freeze-out of charged-particle reactions with such entropies for $Y_e = 0.45$. Then the abundance pattern is not reflecting neutron-separation energies. Possibly more neutron-rich environments with smaller Y_e's could improve this feature, which then do not require (such) high entropies (Meyer 1989, Freiburghaus et al. 1999a).

6.3 Astrophysical sites of the r-process

We have shown in section 6.2 that with the known nuclear properties a site-independent approach, based on a superposition of neutron densities or entropies, can reproduce the solar system r-process abundance pattern (at least beyond Ba). Low metallicity stellar observations show that one type of astrophysical event is responsible for this main r-process component beyond A=130, while another possibly weaker source fills in the lower mass numbers (see section 7). Now we need to address the question of the related astrophysical sites. The necessary conditions turned out to occur in either high entropy environments, which can be moderately neutron-rich, or low entropy environments, which have to be very neutron-rich. The sites which obviously come into mind are SNe II and neutron-star (merger) ejecta. However, for a historical review of all sites suggested so far see Cowan et al. et al. (1991) and Wallerstein et al. (1997), including cosmological, i.e. big bang, sources (Orito et al. 1997).

If SNe II are also responsible for the solar r-process abundances, given the galactic occurance frequency, they would need to eject about 10^{-5} $M_\odot$ of r-process elements per event (if all SNe II contribute equally). The scenario is based on the so-called "neutrino wind", i.e. a wind of matter from the neutron star surface (within seconds after a successful supernova explosion) is driven via neutrinos streaming out from the still hot neutron star (Woosley et al. 1994, Takahashi et al. 1994, Hoffman et al. 1996, 1997, Qian & Woosley 1996, Meyer et al. 1998, Otsuki et al. 2000).

This high entropy neutrino wind is expected to lead to a superposition of ejecta with varying entropies. The r-process by neutrino wind ejecta of SNe II faces two difficulties: (i) whether the required high entropies for reproducing heavy r-process nuclei can really be attained in supernova explosions has still to be verified (Rampp & Janka 2000, Mezzacappa et al. 2001, Liebendörfer et al. 2001ab, Nagataki & Kohri 2001, Thompson et al. 2001), (ii) the mass region 80–110 experiences difficulties to be reproduced adequately (Freiburghaus et al. 1999a, Wanajo et al. 2001). It has to be seen whether the inclusion of non-standard neutrino properties (McLaughlin et al. 1999) can cure both difficulties or lower Y_e zones can be ejected from SNe II, as recently claimed (Sumiyoshi et al. 2001) from assumed prompt, but probably unrealistic, explosion calculations lacking a proper neutrino transport (see the discussion of recent literature in section 3).

Fig. 4 showed the abundance evolution in the innermost zone of a SNe II simulation (Hauser 2002), based on Liebendörfer et al. (2001a) but with (artificially) reduced neutrino opacities by 60%. This led to larger neutrino luminosities, permitting a successful delayed explosion. Entropies per baryon of up to 50 are attained, which is too small for a strong r-process (Freiburghaus et al. 1999a). However, we see a freeze-out with remaining neutrons, leading to the onset of a (weak?) r-process, indicated by the rise of Ge beyond Ni (Ge is the upper limit of the nuclear network employed in that calculation). This result seems possible as a combination of high entropies and a low Y_e=0.39, but needs further analysis. In any case, we have only indications for a weak r-process. Another supernova related site responsible for the "weak" r-process component (i.e. nuclei with A<130) could also be related to explosive C or He-burning in the outer ejected shells (Thielemann et al. 1979, Wheeler et al. 1998, Truran et al. 2001, Meyer et al. 2000, Rauscher et al. 2001a, Rauscher et al. 2002).

An alternative site for the main component are neutron-star ejecta, like e.g. in neutron star mergers. The binary system, consisting of two neutron stars, looses energy and angular momentum through the emission of gravitational waves and merges finally. Such systems are known to exist; four NS-NS binaries have been detected by now (Thorsett 1996, Lorimer 2001). The measured orbital decay gave the first evidence for the existence of gravitational radiation (Taylor 1994) and indicates timescales of the order of 10^8y or less (dependent on the excentricity of the system). The rate of NS mergers has been estimated to be of the order $10^{-6} - 10^{-4}\mathrm{y}^{-1}$ per galaxy (Eichler et al. 1989, Narayan et al. 1992); more recent estimates (van den Heuvel & Lorimer 1996, Kalogera et al. 2001) tend towards the center of this range ($8 \cdot 10^{-6}\mathrm{y}^{-1}$ per galaxy). A merger of two NS can lead to the ejection of neutron-rich material (Davies et al. 1994, Janka & Ruffert 1996, Baumgarte et al. 1997, Ruffert & Janka 1998,

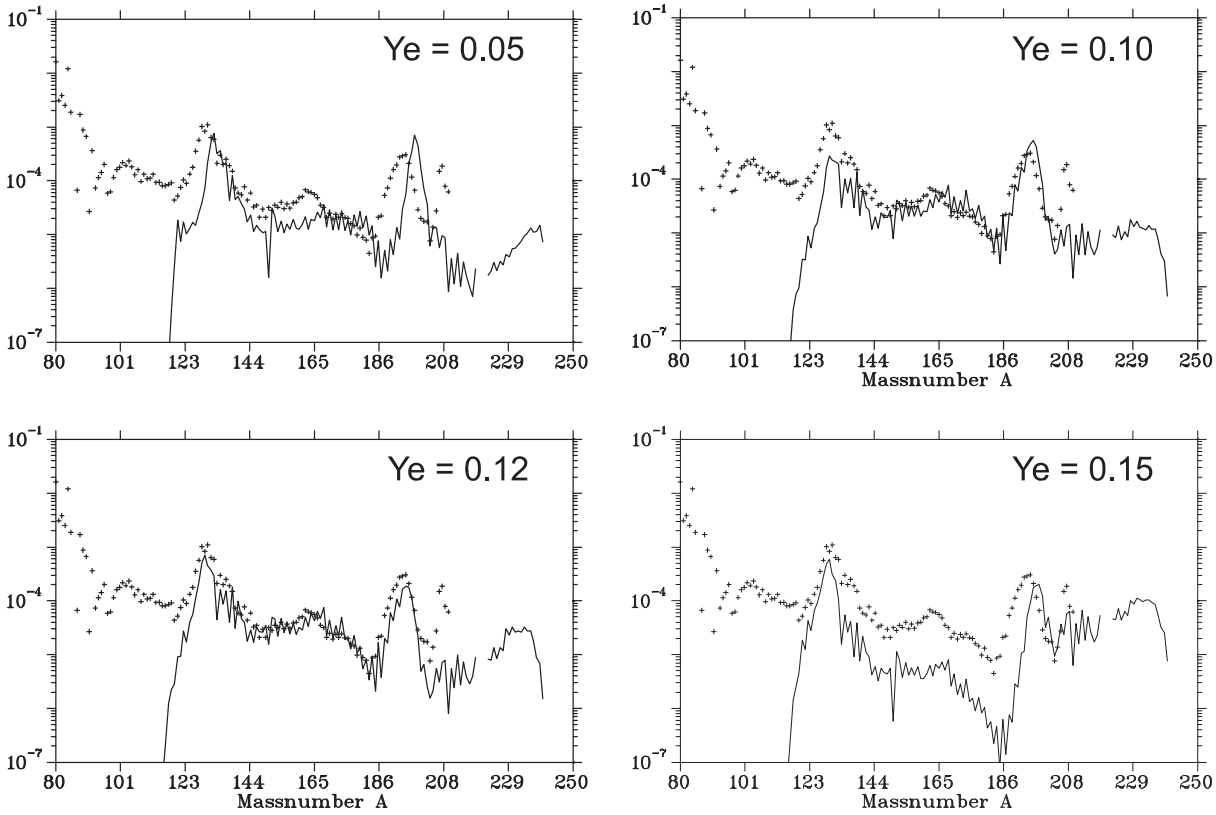

Fig. 16. Calculated r-process distributions for neutron star ejecta with different initial Y_e's. In general one obtains useful contributions for $0.08 < Y_e < 0.15$. A further discussion is given in the text. Y_e determines the total neutron/seed ratio, which is an indication of the strength of the r-process. It affects also the combination of n_n and T, i.e. the r-process path, and therefore the position of peaks. Finally, fission cycling is responsible for the drop of abundances below A=130, but only an improved incorporation of fission barriers and yields will provide the correct abundance distribution in this mass range.

Rosswog et al. 1999, 2000, Ruffert & Janka 2001) of the order of 10^{-2}M$_\odot$ in Newtonian calculations, and could be a promising site for the production of r-process elements. It is even possible that such mergers account for *all* heavy r-process matter in the Galaxy (Lattimer et al. 1977, Eichler et al. 1989, Freiburghaus et al. 1999b, Rosswog et al. 2001). The decompression of cold neutron-star matter has been studied (Lattimer et al. 1977, Meyer 1989), however, a hydrodynamic calculation coupled with a complete r-process calculation has not been undertaken, yet.

Fig. 16 shows the composition of ejecta from a NS merger, dependent on the assumed (not self-consistently modeled) Y_e of the ejecta (Freiburghaus et al. 1999b, Rosswog et al. 2001). It is seen that the large amount of free neutrons (up to n$_n\simeq 10^{32}$ cm^{-3}) available in such a scenario leads to the build-up of the heaviest elements and also to fission cycling within very short timescales, while the flow from the Fe-group to heavier elements "dries up". This leads to a composition void of abundances below the A$\simeq$130 peak, which is, however, dependent on detailed fission yield predictions (Panov et al. 2001). If further observations support such a behavior of Z$<$50 elements in very low metallicity stars (see section 7), it would provide strong support for that type of r-process site, but would definitely require an additional weak astrophysical source which produces the bulk of the lighter r-abundances up to A$\simeq$125. Additional important evidence for the source composition of r-process elements could come from the actinide cosmic ray composition (Westphal et al. 1998, 2001).

At present, these suggested r-process sources, supernovae and neutron star mergers (jets), did not yet prove to be "the" main-component r-process source without reasonable doubt. Self-consistent core collapse supernovae do not give explosions (Ramp & Janka 2000, Mezzacappa et al. 2001, Liebendörfer et al. 2001a, 2002), yet, but parameter studies with neutrino opacities permit to "fit" the correct explosion behavior (Hauser et al. 2002). Thus, there is no way to predict whether the required entropies for an r-process can be obtained (Wanajo et al. 2001, Thompson et al. 2001). Hypernovae (massive stars which end with a central stellar mass black hole rather than a neutron star after supernova explosions) could do so, but their full magneto-hydrodynamic understanding is also not revealed, yet (MacFadyen & Woosley 1999, Cameron 2001ab, MacFadyen et al. 2001). Neutron star merger calculations give the correct mass ejection (Rosswog et al. 1999, 2000), but until now only for non-relativistic calculations. First relativistic merger calculation seem to eject smaller amounts of matter (Oechslin et al. 2002). The abun-

dance predictions for neutron star mergers look excellent (Freiburghaus et al. 1999b), but still take Y_e as a free parameter rather than treating weak interactions and neutrino transport self-consistently.

7 Observational Constraints and Galactic Evolution

7.1 Observations of individual sources

Explosive nucleosynthesis yields leave fingerprints in observations of individual stellar events as well as their remnants via spectra, lightcurves, X-rays and radioactivities/decay gamma-rays (see e.g. the discussions in Thielemann et al. 1996, 2000, Iwamoto et al. 1999).

^{56,57}Ni and ^{44}Ti abundances, and possibly stable Ni/Fe ratios in SNe II, give insight into the details of the explosion mechanism with respect to the mass cut between the neutron star and the SN ejecta, the total energy of the explosion, the entropy and the Y_e in the innermost ejecta (see section 3). The intermediate mass elements Si-Ca provide information about the explosion energy and the stellar structure of the progenitor star, while elements like O, Ne and Mg are essentially determined by the stellar progenitor evolution. Therefore, only the correct reproduction of Fe-group abundances are a direct test whether one understands the explosion mechanism (Thielemann et al. 2001).

In SNe Ia, the ^{56}Ni production and the Si-Ca/Fe ratio are related to the total explosion energy and burning front speed in layers of the exploding white dwarf. Constraints on the ignition density and burning front speed in the central regions (as discussed in section 4) are reflected e.g. in minor isotopic abundances like ^{50}Ti and ^{54}Cr, where direct supernova or remnant observations cannot be used. Here one can only make use of global abundance constraints from galactic evolution, which therefore permit only statements about an "average" SN Ia. The application of present day electron capture rates makes it hard to account for our solar system ^{48}Ca (Brachwitz et al. 2002). On the other hand, observations of varying stable Ni/Fe ratios during the evolution of a supernova (by spectral means) related to ^{54}Fe and ^{58}Ni, might give clues to the metallicity of the exploding white dwarf (Höflich et al. 1998).

Observations of nova ejecta support the features discussed in section 5 (Truran 1998), while the spectral resolution of new X-ray observatories can help to put constraints on X-ray burst models. So far, there have been no direct observations of (rare) r-process elements in individual explosions, but the cosmic-ray source composition of actinides (Westphal et al. 1998, 2001) might provide specific clues.

7.2 Galactic evolution

Opposite to individual source observations, galactic evolution can serve as a global test for all contributing stellar yields, i.e. especially intermediate and low mass stars through planetary nebula ejection, mass loss from massive stars, as well as the ejecta of SNe II and SNe Ia (for details see e.g. Tsujimoto et al. 1995, Thomas et al. 1998, Matteucci et al. 1999, Chiappini et al. 1999). The composition of interstellar gas in galaxies as well as clusters of galaxies can serve the same purpose (Finoguenov et al. 2002). Here we want to focus on specific observational clues to SNe Ia and SNe II nucleosynthesis and indicate how very low metallicity stars might witness individual rather than only integrated SNe II yields.

Stars (with understood exceptions) do not change the surface composition during their evolution. Thus, surface abundances reflect the interstellar medium (ISM, out of which the stars formed) at the time of their formation. Therefore, observations of the surface composition (via spectra) of stars over a variety of ages and metallicities give a clue to gas abundances throughout the evolution of our Galaxy.

Very old (low metallicity) stars witness very early galactic evolution and thus fast evolving massive stars, i.e. SNe II nucleosynthesis, seen in an enhancement of the alpha elements (O through Ca) in comparison to Fe for [Fe/H]=$\log_{10}$ [(Fe/H)/(Fe/H)$_\odot$] <-1 (Gratton & Sneden 1991, Nissen et al. 1994, Argast et al. 2000, 2001). The higher ratio of Fe-group elements to Si-Ca in SNe Ia, appearing later in galactic evolution, has to compensate for these overabundances in SNe II in order to obtain solar abundance ratios for the combined nucleosynthesis products at solar metallicity [Fe/H]=0.

The Fe-group ejecta of both types of supernovae have to differ because Ti/Fe and Mn/Fe are found above, or respectively below, solar ratios in SNe II, requiring the opposite behavior of SNe Ia (Iwamoto et al. 1999). At very low metallicities Cr, Mn, and Co show peculiar features, possibly related to the progenitor mass dependence of SNe II (Nakamura et al. 1999).

Recent promising trends in galactic evolution modeling might provide constraints on individual supernova models rather than only global properties of SNe II and SNe Ia. The reason for this possibility is the fact that there is no instantaneous mixing of ejecta with the interstellar medium, and therefore early phases of galactic evolution can present a connection between low metallicity star observations and a single supernova event. On average, each supernova pollutes a volume of the interstellar medium containing $\approx (3-5) \times 10^4 M_\odot$. (for references see e.g. Argast et al. 2000). Each volume of the interstellar medium containing $\approx 3 \times 10^4 M_\odot$ needs to be enriched by $\approx 10^3$ SNe in order to obtain solar metallicities.

After a supernova polluted such a previously pristine environment mass, it results in values for [x/Fe] and [Fe/H] in the remnant, x standing for any element. Variations in SN II properties as a function of progenitor mass (and metallicity) should lead to a scatter in [x/Fe] for the same [Fe/H]. The amount of the polluted volume depends on the explosion energy, and if there is a strong variation of explosion energies with progenitor mass this could affect the relation between [x/Fe] and the metallicity [Fe/H] (Nakamura et al. 1999). The scatter in [x/Fe] expected for the same [Fe/H] is observed up to metallicities of [Fe/H]=-2, where it vanishes because overlapping contributions from many SNe II behave

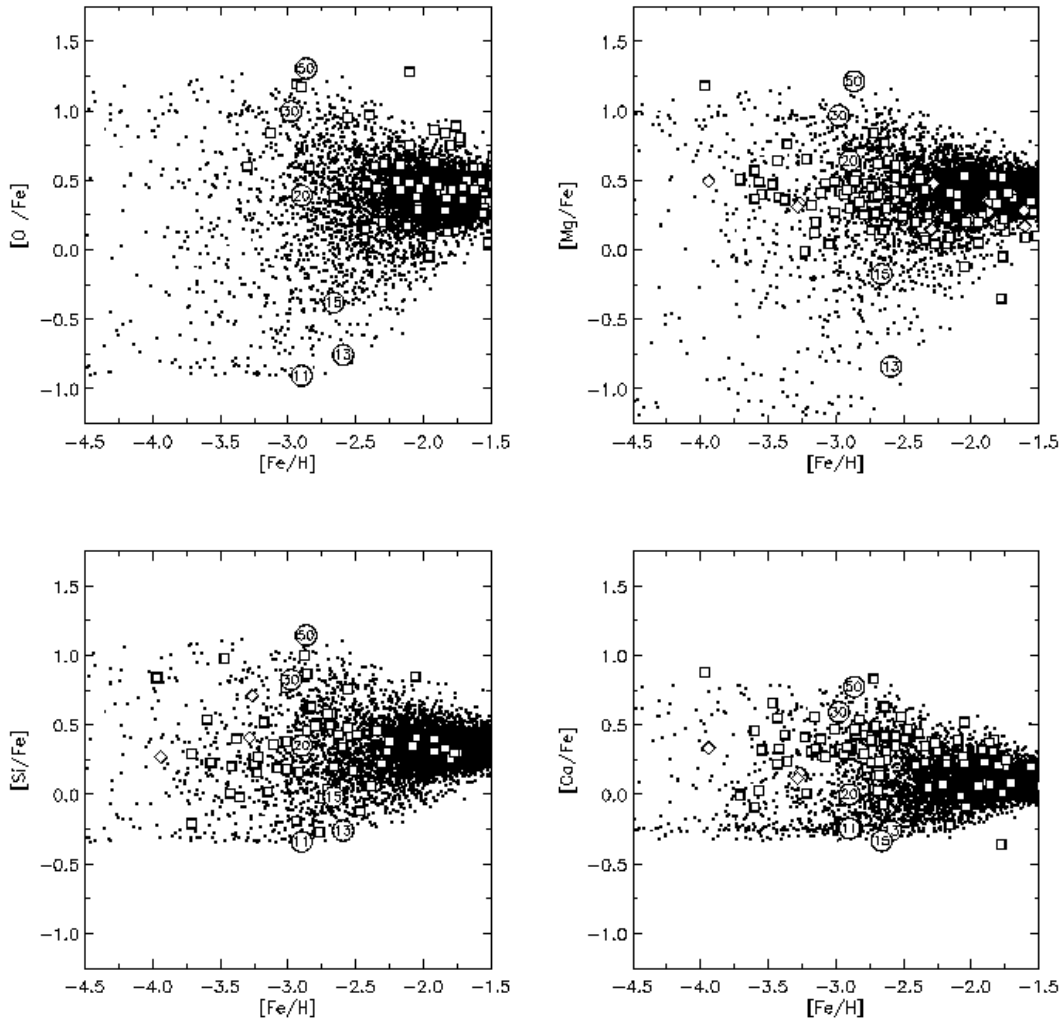

Fig. 17. Comparison of low metallicity observations with SN II yields and a galactic evolution model. Three types of symbols are given, circles, squares and dots. The *squares show observations* of low metallicity stars with a scatter at very low metallicities. The *open circles* indicate the x/Fe and Fe/H ratios in a volume of $5 \times 10^4 M_\odot$ of an initially pristine (big bang) composition, polluted by *single supernovae* with our ejecta compositions. The numbers inside the circles refer to the progenitor mass of a supernova whose ejecta composition was mixed with $5 \times 10^4 M_\odot$ of prestine ISM. The (galactic evolution) *model stars are indicated by dots* (see the text for a detailed discussion).

like a well mixed medium (Argast et al. 2000, 2001).

Some results from such an approach (Argast et al. 2000, 2001) are displayed in Fig. 17 which shows O/Fe, Mg/Fe, Si/Fe and Ca/Fe ratios. Three types of symbols are given, circles, squares and dots. The squares show observations of low metallicity stars with a scatter at very low metallicities, as expected if mixing of ejecta with the ISM is not instantaneous and contributions from individual supernovae with different progenitor masses give their different signatures. This scatter apparently becomes as small as the observational uncertainties at [Fe/H]=-2, where everywhere in the ISM the average signature of SNe II yields emerges due to an integration over the progenitor mass distribution (initial mass function, IMF). The open circles indicate the x/Fe and Fe/H ratios in a volume of $5 \times 10^4 M_\odot$ of an initially pristine (big bang) composition, polluted by a single supernova with our ejecta compositions (Thielemann et al. 1996, Nomoto et al. 1997). The numbers inside the circles refer to the progenitor mass of a supernova whose ejecta composition was mixed with $5 \times 10^4 M_\odot$ of prestine ISM. Such a remnant would therefore show directly the [Fe/H] metallicity caused by a single SN event. However, we compare with observations from low metallicity stars rather than remnants. The model stars are indicated by dots (Argast et al. 2000, 2001). They assume a stochastic star formation at random positions in the ISM and with random progenitor masses (however, with a statistical distribution according to a Salpeter IMF). One sees on the one hand that much smaller contributions to a stellar progenitor can be possible than expected from a single remnant (leading to Fe/H ratios much smaller than given in the circles). On the other hand, successive enrichment of many (and finally overlapping) remnants leads to a metallicity evo-

lution which approaches at [Fe/H]=-2 the IMF-averaged SNe II yields. These are apparently in agreement with the observations.

The features (at [Fe/H]=-2) agree nicely with previous galactic evolution calculations which applied our yields (Tsujimoto et al. 1995, Thomas et al. 1998, Matteucci et al. 1999, Chiappini et al. 1999), assuming instantaneous mixing of yields with the ISM. However, the observed and predicted scatter at very low metallicities bears information which was previously unavailable. (This approach relies on the assumption that these difficult low metallicity observations are correct.) The scatter for Si and Ca/Fe seems essentially correct, possibly only slightly too large, which could indicate that the lower mass SNe II (11 and 13 $M_\odot$) produce slightly too small ratios and the high mass end (50 $M_\odot$) slightly too large ones. This can be related to the uncertainty of the mass cut and the assumptions made on the Fe-yields as a function of progenitor mass.

Thus, while the average x/Fe is correct, the progenitor mass dependence of the Fe-yields could be slightly too strong. This is, however, a small effect for the elements Si and Ca, produced in explosive burning. Much larger deviations can be seen for O and Mg, which are dominated by uncertainties in stellar evolution (not the explosion). Here the lower mass stars (11, 13, 15 $M_\odot$) predict clearly much too small ratios, far beyond the observational scatter, while the 50 $M_\odot$ model predicts slightly too large ones. This indicates a problem in the stellar models which might improve with more recent calculations (Chieffi et al. 1998, Umeda et al. 2000, Heger et al. 2000ab, Limongi et al. 2000) and has to be tested. The main conclusion we can draw from these results is that such investigations can also test individual stellar yields rather than only IMF integrated samples. This is a large advantage over the very few data points we have from individual supernova observations.

Such tests seem also very useful for other applications, where one is (i) not certain about the stellar site of a nucleosynthesis product or (ii) about contributions from objects with different evolution timescales. The possible influence of hypernova contributions, objects beyond the SN II mass scale which lead to a central black hole but still cause an explosion (Nakamura et al. 2001), and very massive stars with several 100 $M_\odot$, which undergo a complete disruption by nuclear burning (VMOs, Heger & Woosley 2002), should be considered in a similar way. In the latter case a full understanding of the initial mass function, describing the formation frequency as a function of progenitor mass, is, however, still marginal.

The r-process is an example where the alternative site to supernovae, neutron star mergers, occur with a much smaller frequency. In that case, the mixed phase (orrurring for SNe II at about [Fe/H]=-2) should be delayed to larger metallicities. In addition, one expects with the large amounts of r-process ejecta from each occasionally occurring neutron star merger (Freiburghaus et al. 1999b) a much larger scatter than for the smoothly changing supernova yields as a function of stellar mass. Both effects are seen in the r/Fe observations (a scatter of almost a factor of 1000 (Sneden et al. 2000, Cayrel et al. 2001) at low metallicities, which still amounts to about a factor of 10 at [Fe/H]=-1. Combined with the suppression of abundances below A=130 in low-metallicity stars, this could be taken as supportive features for a fission cycling r-process. This would also apply, even if some specific type of supernova is responsible. Similar galactic evolution calculations as presented here are needed in order to test the expected amount of scatter as a function of metallicity to give clues on the r-process site. The implications for possible r-process site(s) have been discussed in (Freiburghaus et al. 1999b, Qian 2000, Cameron 2001ab, Rosswog 2001, Thielemann et al. 2002, Qian & Wasserburg 2002).

References

Ahmad QR, Allen RC, Andersen TC, et al. 2001, Phys. Rev. Lett. 87, 1301

Argast, D., Samland, M., Gerhard, O.E., Thielemann, F.-K. 2000, A & A 356, 873

Argast, D., Samland, M., Thielemann, F.-K., Gerhard, O.E. 2001, submitted to A&A

Arnett, W.D., Thielemann, F.-K. 1985, Ap. J. 295, 589

Asida, S. M., Arnett, W.D. 2000, ApJ 545, 435

Aufderheide, M., Baron, E., Thielemann, F.-K. 1991, Ap. J. 370, 630

Bahcall JN, Pinsonneault MH, Basu S 2001, ApJ 555, 990

Baumgarte, T.W., Cook, G.B., Scheel, M.A., Shapiro, S.L. 1997, Phys. Rev. Lett. 79, 1182

Bethe, H.A. 1990, Rev. Mod. Phys. 62, 801

Brachwitz, F. et al. 2000, Ap. J., 536, 934

Brachwitz, F. (et al.) 2002, Ph. D. thesis, Univ. of Basel and in preparation

Burbidge, E.M., Burbidge, G.R., Fowler, A.A., Hoyle, F. 1957, Rev. Mod. Phys. 29, 547

Burrows, A. 1990, Ann. Rev. Nucl. Part. Sci. 40, 181

Busso M, Gallino R, Lambert DL, Travaglio C, Smith VV 2001, Ap. J. 557, 802

Cameron, A.G.W. 1957, Atomic Energy of Canada, Ltd., CRL-41

Cameron, A.G.W. 2001a, Nucl. Phys. A688, 289c

Cameron, A.G.W. 2001b, ApJ 562, 456

Cayrel, R. et al. 2001, Nature 409, 691

Charbonnel C, Dappen W, Schaerer D, et al. 1999, A&AS 135, 405

Chen, B., Dobaczewski, J., Kratz, K.-L., Langanke, K., Pfeiffer, B., Thielemann, F.-K., Vogel, P. 1995, Phys. Lett., B355, 37

Chiappini, C., Matteucci, F., Beers, T. C., Nomoto, K. 1999, ApJ 515, 226

Chieffi, A., Limongi, M., Straniero, O. 1998, Ap. J. 502, 737

Coc, A., Hernanz, M., José, J., Thibaud, J.P. 2000, A & A 357, 561

Costa V, Rayet M, Zappala RA, Arnould M 2000, A & A 358, L67

Cowan, J. J., Thielemann, F.-K., Truran, J. W. 1991, Phy. Rep., 208, 267

Cowan, J.J., Pfeiffer, B., Kratz, K.-L., Thielemann, F.-K., Burles, S., Tytler, D. 1999, Ap. J. 521, 194

Cumming A, Bildsten L 2001, Ap. J. Letters 559, L127

Davies, M.B., Benz, W., Piran, T., Thielemann, F.-K. 1994, Ap.

J. 431, 742
Dominguez, I., Höflich, P., Straniero, O. 2001a, Ap. J. 557, 279
Dominguez I, Abia C, Straniero O, Chieffi A, Limongi M 2001b, Astrophys. Space Sci. Suppl. 277, 161
Eichler, D., Livio, M., Piran, T., Schramm, D. N. 1989, Nature, 340, 126
Finoguenov, A., Matsushita, K., Böhringer, H., Ikebe, Y., Arnaud, M. 2002, A & A 381, 21
Fisker, J.L. et al. 2001a, At. Data Nucl. Data Tables 79, 1
Fisker, J.L., Rembges, F., Barnard, V., Wiescher, M. 2001b, in *The Influence of Binaries on Stellar Population Studies*, ed. D. Vanbeveren, Kluwer Academic Publishers, p. 569
Freiburghaus, C. et al. 1999a, Ap. J. 516, 381
Freiburghaus, C., Rosswog, S., Thielemann, F.-K. 1999b, Ap. J. 525, L121
Fuller, G.M., Fowler, W.A., Newman, M. 1985, Ap. J. 293, 1
Görres, J., Wiescher, M., Thielemann, F.-K. 1995, Phys. Rev. C51, 392
Goriely, S., Arnould, M. 1996, A & A, 312, 327
Gratton, R.G., Sneden, C. 1991, A & A 241, 501
Grevesse, N., Sauval, A.J. 1998, Space Sci. Rev. 85, 161
Hashimoto, M., Iwamoto, K., Nomoto, K., 1993, Ap. J. 414, L105
Hauser, P. (et al.) 2002, Master Thesis Univ Basel and in preparation
Heger, A., Langer, N., Woosley, S.E. 2000a, Ap. J., 528, 368
Heger, A., Langer, N. 2000b, Ap. J., 544, 1016
Heger, A., Langanke, K., Martinez-Pinedo, G., Woosley, S.E. 2001a, Phys. Rev. Lett 86, 1768
Heger, A. Woosley, S.E., Martinez-Pinedo, G., Langanke, K. 2001b, ApJ 560, 307
Heger, A. Woosley, S.E. 2002, ApJ, in press
Hillebrandt, W., Niemeyer, J.C. 2000, Ann. Rev. of Astron. Astrophys. 38, 191
Hix, W.R., Thielemann F.-K. 1996, Ap. J. 460, 869
Hix, W.R., Thielemann F.-K. 1999, Ap. J. 511, 862
Höflich, P. 2000, in *Type Ia Supernovae, Theory and Cosmology*, eds. J.C. Niemeyer, J.W. Truran, Cambridge University Press, p.89
Höflich, P., Khokhlov, A. 1996, Ap. J., 457, 500
Höflich, P., Wheeler, J.C., & Thielemann, F.-K. 1998, ApJ 495, 617
Hoffman, R.D. Woosley, S. E., Fuller, G. M., Meyer, B. S. 1996, Ap. J. 460, 478
Hoffman, R.D. Woosley, S. E., Qian, Y.-Z. 1997, Ap. J. 482, 951
Hoffman RD, Woosley SE, Weaver TA, Rauscher T, Thielemann FK 1999, Ap. J. 521, 735
Iliadis, C., Endt, P.M., Prantzos, N., Thompson, W.J. 1999, Ap. J. 524, 434
Iwamoto, K. et al. 1999, Ap. J. Suppl. 125, 439
Janka, H.T., Ruffert, M. 1996, A&A 307, L33
José, J., Coc, A., Hernanz, M. 1999, Ap. J. 520, 342
José, J., Coc, A., Hernanz, M. 2001, Ap. J. 560, 897
Käppeler, F., Beer, H., Wisshak, K. 1989, Rep. Prog. Phys. 52, 945
Käppeler, F., Wiescher, M., Thielemann, F.-K. 1998, Ann. Rev. Nucl. Part. Sci. 48, 175
Käppeler, F. 1999, Prog. Part. Nucl. Phys. 43, 419
Kalogera, V., Narayan R, Spergel DN, Taylor JH 2001, Ap. J. 556, 340
Keil, W., Janka, H.-T. 1995, A & A 296, 145
Kifonidis, K., Plewa, T., Janka, H.-T., Müller, E. 2000, ApJ 531, L123
Kratz, K.-L., Bitouzet, J.-P., Thielemann, F.-K., Möller, P., Pfeiffer, B. 1993, Ap. J. 402, 216
Kratz, K.-L., Pfeiffer, B., Thielemann, F.-K., 1998, Nucl. Phys. A630, 352c
Kratz, K.-L., Pfeiffer, B., Thielemann, F.-K., Walters, W.B. 2000, Hyperfine Interactions 129, 185
Langanke, K., Martinez-Pinedo, G. 2000, Nucl. Phys. A673, 481
Langer, N., Fliegner, J., Heger, A., Woosley, S.E. 1997, Nucl. Phys. A621, 457c
Lattimer, J. M., Mackie, F., Ravenhall, D. G., Schramm, D. N. 1977, Ap. J., 213, 225
Leibundgut, B. 2001, Ann. Rev. Astron. Astrophys. 39, 67
Lewin, W.H.G., van Paradijs, J., Taam, R.E. 1993, Space Sci. Rev. 62, 223
Liebendörfer, M. et al. 2001a, Phys. Rev. D 6310, 3004
Liebendörfer, M., Mezzacappa, A., Thielemann, F.-K. 2001b, Phys. Rev. D 6310, 4003
Liebendörfer M, Messer OEB, Mezzacappa A, Hix WR 2002, in Proceedings of the 20th Texas Symposium on Relativistic Astrophysics, eds. J.C. Wheeler & H. Martel, American Institute of Physics, in press
Limongi, M., Straniero, O., Chieffi, A. 2000, ApJSS 129, 625
Livio, M. 2001, in *Supernovae and Gamma-Ray Bursts: The Biggest Explosions since the Big Bang*, eds. M. Livio, N. Panagia, K. Sahu, Cambridge Univ. Press, p.334
Lorimer, D.R. 2001, Living Reviews in Relativity, in press
MacFadyen AI, Woosley SE 1999, Ap. J. 524, 262
MacFadyen AI, Woosley SE, Heger A 2001, Ap. J. 550, 410
Maeder, A., Meynet, G. 2000a, A&A 361, 159
Maeder, A., Meynet, G. 2000b, ARA&A 38, 143
Maeder, A., Meynet, G. 2001, A&A 372, 555
Martinez-Pinedo, G., Langanke, K., Dean, D.J. 2000, ApJS, 126, 493
Matteucci, F., Romano, D., Molaro, P. 1999, A&A 341, 458
McLaughlin, G.C. et al. 1999, Phys. Rev. C59, 2873
Meynet, G., Maeder, A. 2000, A&A 361, 101
Meyer, B. S. 1989, Ap. J. 343, 254
Meyer BS, McLaughlin GC, Fuller GM 1998, Phys. Rev. C58, 3696
Meyer, BS, Clayton DD, The LS 2000, Ap. J. 540, L49
Mezzacappa A, Calder AC, Bruenn SW, Blondin JM, Guidry MW, Strayer MR, Umar AS 1998, Ap. J. 495, 911
Mezzacappa, A. et al. 2001, PRL 86, 1935
Nagataki, S., Kohri, K. 2001, Publ. Astron. Soc. Japan 53, 547
Nakamura, T. et al. 1999, Ap. J. 517, 193
Nakamura, T. et al. 2001, Ap, J. 555, 880
Narayan, R., Paczynski, B., Piran, T., 1992, Ap. J. 395, L83
Niemeyer, J.C. 1999, Ap. J. 523, L57
Nissen, P.E. et al. 1994, A&A 285, 440
Nomoto, K., Hashimoto, M. 1988, Phys. Rep. 163, 13
Nomoto, K. et al. 1997, Nucl. Phys., A161, 79c
Nomoto, K., Thielemann, F.-K., Yokoi, K. 1984, Ap. J. 286, 644
Nomoto, K. et al. 2000, in *Type Ia Supernovae: Theory and Cosmology*, Cambridge Univ. Press, eds. J.C. Niemeyer, J.W. Truran, p.63
Nugent, P. et al. 1997, Ap. J. 485, 812
Oechslin, R., Rosswog S., Thielemann, F.-K. 2002, Phys. Rev. D, in press
Orito M, Kajino T, Boyd RN, Mathews GJ 1997, Ap. J. 488, 515
Otsuki, K. et al. 2000, Ap. J. 533, 424

Panov I, Freiburghaus C, Thielemann F-K 2001, Nucl. Phys. A688, 587
Pearson, J. M., Nayak, R. C., Goriely, S. 1996, Phys. Lett. B387, 455
Pfeiffer B, Kratz KL, Thielemann FK, Walters WB 2001, Nucl. Phys. A693, 282
Prakash M, Lattimer JM, Sawyer RF, Volkas RR 2001, Ann. Rev. Nucl. Part. Sci. 51, 295
Qian, Y.-Z., Woosley, S. E. 1996, Ap. J., 471, 331
Qian, Y.-Z. 2000, Ap. J. 534, L67
Qian, Y.-Z., Wasserburg, G.J. 2002, Ap.J., in press (astro-ph/0110532)
Rampp, M., Janka, H.T. 2000, Ap. J. 539, L33
Rauscher, T., Rembges, F., Schatz, H., Wiescher, M., Thielemann, F.-K. 2000, in *The beta Decay, from Weak Interaction to Nuclear Structure*, eds. P. Dessagne, A. Michalon, C. Miehé, IRes Strasbourg, p. 51
Rauscher, T., Heger, A., Hoffman, R.D., Woosley, S.E. 2001a, Nucl. Phys. A 688, 193
Rauscher, T., Hoffman, R.D., Heger, A., Woosley, S.E. 2001b, in *Hadrons, Nuclei, and Applications*, eds. G.C. Bonsignori, M. Bruno, A. Ventura, D. Vretenar, World Scientific, p. 277 (nucl-th/0008065)
Rauscher, T., Heger, A., Hoffman, R.D., Woosley, S.E. 2002, ApJ, in press (astro-ph/0112478)
Rehm, E. et al. 1998, Phys. Rev. Lett. 80, 676
Rembges, F., Freiburghaus, C., Rauscher, T., Thielemann, F.-K., Schatz, H., Wiescher, M. 1997, Ap. J. 484, 412
Rembges, F. 1999, Ph.D. thesis, Univ. Basel, unpublished
Renzini, A., Voli, M. 1981, A & A 94, 175
Riess, A.G. et al. 2000, Ap. J. 536, 62
Rosner, R., Alexakis, A., Young, Y.-N., Truran, J. W.; Hillebrandt, W. 2001, Ap. J. Letters 562, L177
Rosswog, S., Liebendörfer, M., Thielemann, F.-K., Davies, M., Benz, W., Piran, T. 1999, A&A 341, 499
Rosswog, S., Davies, M. Thielemann, F.-K., Piran, T. 2000, A&A 360, 171
Rosswog, S.K., Freiburghaus, C., Thielemann, F.-K. 2001., Nucl. Phys. A688, 344
Ruffert, M., Janka, H.-T. 1998, A&A 338, 535
Ruffert, M., Janka, H.-T. 2001, A&A 380, 544
Schatz, H. et al. 1998, Phys. Rep. 294, 167
Schatz H et al. 2001, Phys. Rev. Lett. 86, 3471
Sneden, C. et al. 2000, Ap. J. 533, L139
Starrfield, S. 1999, Phys. Rep. 311, 371
Starrfield, S., Sparks, W. M., Truran, J. W., Wiescher, M. C. 2000, Ap. J. Suppl. 127, 485
Suess, H.E. & Urey, H.C. 1956, Rev. Mod. Phys. 28, 53
Sumiyoshi K, Terasawa M, Mathews GJ, et al. 2001, ApJ 562, 880
Taam, R.E. 1985, Ann. Rev. Nucl. Part. Sci. 35, 1
Taam, R.E., Woosley, S.E., Lamb, D.Q. 1996, Ap. J. 459, 271
Takahashi, K., Witti, J., Janka, H.-T. 1994, A&A, 286, 857
Taylor, J. 1994, Rev. Mod. Phys. 66, 711
Thielemann, F.-K., Arnould, M. Hillebrandt, W. 1979, A&A 74, 175
Thielemann, F.-K., Arnett, W.D. 1985, Ap. J. 295, 604
Thielemann, F.-K., Nomoto, K., & Yokoi, K. 1986, A&A 158, 17
Thielemann, F.-K., Arnould, M., Truran, J. W. 1987, in *Advances in Nuclear Astrophysics*, ed. E. Vangioni-Flam, Gif sur Yvette, Editions Frontière, p.525
Thielemann, F.-K., Hashimoto, M., Nomoto, K. 1990, Ap. J. 349, 222
Thielemann, F.-K., Bitouzet, J.-P., Kratz, K.-L., Möller, P., Cowan, J. J., Truran, J. W. 1993, Phys. Rep., 227, 269
Thielemann, F.-K., Kratz, K.-L., Pfeiffer, B., Rauscher, T., van Wormer, L., & Wiescher, M. C. 1994, Nucl. Phys. A570, 329c
Thielemann, F.-K., Nomoto, K., Hashimoto, M. 1996, Ap. J. 460, 408
Thielemann, F.-K. 2000, in *Astronomy with Radioactivities*, eds. R. Diehl, D. Hartmann, MPE Report, p. 123
Thielemann, F.-K. et al. 2001, in *The Largest Explosions Since the Big Bang: Supernovae and Gamma-Ray Bursts*, eds. M. Livio, N. Panagia, K. Sahu, Cambridge University Press, p.258
Thielemann, F.-K. et al. 2002, Space Sci. Rev., in press
Thomas, D., Greggio, L., Bender, R. 1998, MNRAS 296, 119
Thompson, T.A., Burrows, A., Meyer, B.S. 2001, Ap. J. 562, 887
Thorsett, S.E. 1996, Phys. Rev. Lett. 77, 1432
Truran, J.W. 1998, in Proc. *9th Workshop on Nuclear Astrophysics*, eds. W. Hillebrandt, E. Müller, Max-Planck-Institut f. Astrophysik, p.107
Truran, J.W. et al. 2000, in *The First Stars*, Springer, eds. A. Weiss et al.
Truran, J.W. et al. 2001, Nucl. Phys. A688, 330
Tsujimoto, T. et al. 1995, MNRAS 277, 945
Umeda, H., Nomoto, K., Nakamura, T. 2000, in *The First Stars*, Springer, eds. A. Weiss, T.G. Abel, V. Hill, Springer Verlag
van den Bergh, S., & Tammann, G. 1991, ARA&A 29, 363
van den Heuvel, E.P.J., Lorimer, D.R. 1996, MNRAS 283, L37
van den Hoek, L.B., Groenewegen, M.A.T. 1997, A & AS 123, 305
Van Eck S, Goriely S, Jorissen A, Plez B 2001, Nature 412, 793
Wallerstein, G. et al. 1997, Rev. Mod. Phys. 69, 995
Wanajo, S. et al. 2001, Ap. J. 554, 578
Westphal, A. J., Weaver, B. A., Tarl, G. 2001, Advances in Space Research 27, 797
Westphal, A.J., Price PB, Weaver BA, Afanasiev VG 1998, Nature 396, 50
Wheeler JC , Cowan JJ, Hillebrandt W 1998, Ap. J. 493, L101
Wiescher, M., Görres, J., Schatz, H. 1999, J. Phys. G. 25, R133
Wiescher, M., Schatz, H. 2000, Prog. Theor. Phys. Supp. 140, 11
Wiescher, M. et al. 2002, EPJ, in press
Woosley SE, Howard WM 1978, Ap. J. Suppl. 36, 285
Wilson, J.R., Mayle, R.W. 1993, Phys. Rep. 227, 97
Woosley, S.E., Weaver, T.A. 1986, Ann. Rev. Astron. Astrophys. 24, 205
Woosley, S.E., Weaver, T.A. 1994, in *Les Houches, Session LIV, Supernovae*, eds. S.R. Bludman, R. Mochkovitch, J. Zinn-Justin, Elsevier, p. 63
Woosley, S.E. et al. 1994, Ap. J. 433, 229
Woosley, S.E., Weaver, T.A. 1995, Ap. J. Suppl. 101, 181
Woosley, S.E. 1997, Ap. J. 476, 801